Combustion and Flame 271 (2025) 113841

Contents lists available at ScienceDirect

Combustion and Flame

journal homepage: www.sciencedirect.com/journal/combustion-and-flame

Combustion kinetics of alternative fuels, Part-IV: Extending reaction mechanism "DLR Concise" to include oxygenates components

Trupti Kathrotia [a,*], Thomas Bierkandt [a], Nina Gaiser [a], Sandra Richter [a], Fabian Lindner [a,b], Sascha Jacobs [a], Clemens Naumann [a], Torsten Methling [a], Patrick Oßwald [a], Markus Köhler [a]

[a] Institute of Combustion Technology, German Aerospace Center (DLR), 70569 Stuttgart, Germany
[b] University of Stuttgart, Institute of Combustion Technology for Aerospace Engineering, Stuttgart, Germany

ARTICLE INFO

Keywords:
Polyoxymethylene dimethyl ethers (OME / PODE / PODME)
Oxygenates
Transportation fuels
Reaction mechanism
Fuel assessment

ABSTRACT

In our previous work on hydrocarbons (Kathrotia et al., Fuel 2021;302:120736) and jet fuels (Kathrotia et al., Fuel 2021;302:120737) the molecular fuel composition was shown to be an important aspect of understanding the fuel combustion chemistry and, more importantly, the emission behavior. In this extension, we elaborate our high-temperature jet fuel surrogate reaction mechanism (referred hereafter as DLR Concise) to include the chemical class of oxygenated hydrocarbons for transportation fuels. These oxygen containing species have been widely investigated in ground transportation fuels. With DLR Concise we aim for a flexible reaction model for alternative fuel surrogates; a single reaction model with the target application to both aviation- as well as transportation-fuels.

The main focus of this work is to describe the reaction kinetics of oxymethylene ethers (OME_x, x = 0–5) in low to high temperatures. OMEs are promising alternative fuels that can be derived from a variety of sustainable sources. The absence or reduction of C-C bonds makes them attractive for the reduction of soot precursors and soot emissions. The reaction model of OMEs presented in this work is extensively validated against wide-ranging experiments both in-house and from literature. The main purpose of the DLR Concise is to provide a reaction mechanism with a large degree in flexibility to simulate various fuel surrogates (existing and new) and predict pollutants for the fuel assessment based on fuel molecular structure.

A comprehensive model validation as well as new in-house experimental data set on C_1-C_4 alcohols and primary reference fuel (PRF90) measured in high-temperature flow reactor is available as supplemental material.

1. Introduction

Synthetic fuels from renewable sources are poised to play a crucial role in the future of sustainable transportation. In response to environmental concerns and the irreversible impacts of climate change, many countries are moving away from conventional fossil fuels. Large economies are prioritizing electrified vehicles and renewable fuels in their short- to mid-term goals. However, not all transportation applications can be easily electrified. For heavy-duty transportation, haulage, and specialized vehicles, synthetic fuels offer a viable alternative. These fuels not only help reduce carbon footprints but also contribute to pollutant reduction, with synthetic oxygenated fuels showing potential in lowering hydrocarbon and soot emissions, though with an increase in carbonyl containing emissions [1–3].

Polyoxymethylene dimethyl ethers or oxymethylene ethers, (OMEs), are long chain compounds with molecular formula $CH_3O(\text{-}CH_2O\text{-})_xCH_3$, containing repetitive central -CH_2O- units. The nomenclature of OMEs (used as general class) hereafter is depicted as OME_x, where typically x = 0–5 with dimethyl ether (DME or OME_0) considered as the smallest OME. They are regarded as important alternative synthetic fuels (e-fuels) due to their production from biomass or through sustainable power-to-liquid (PtL) technologies [3–9] as well as their potential to improve carbon containing pollutants formations [10]. The presence of about half of the C-O bonds compared to C-H bonds in their respective hydrocarbons makes OMEs attractive for reducing soot emissions. Here, chemical kinetics play a vital role in understanding these phenomena and enable future assessment strategies [11].

In recent years, significant scientific work has focused on technological advancement in OME production and their combustion characteristics, closely linked to emission reductions studies in various engine

* Corresponding author at: German Aerospace Center, Pfaffenwaldring 38-40, 70569 Stuttgart, Germany.
E-mail address: trupti.kathrotia@dlr.de (T. Kathrotia).

https://doi.org/10.1016/j.combustflame.2024.113841
Received 28 May 2024; Received in revised form 31 October 2024; Accepted 3 November 2024
Available online 17 November 2024

geometries: A review on recent advances in reaction kinetics is available in [8]. Most of the investigations on OMEs published before 2015 were mainly dedicated to the OME0 [12–15], which is supplemented by many more since then [16–18]. The first ignition delay time measurements of neat OME1 were published in [19] which has been extended by experimental as well as modeling efforts, to cite a few [20–26]. However, studies on larger OMEs remain limited [27–35]. The investigations on OMEs include studies on fundamental combustion characteristics of ignition delay times [16,19,25,30–33,36], flame speeds [32,33] or burning velocities [27,37], as well as speciation in reactors [14,18,20,23,35,38–44] and in laminar flames [27,34,45–47], helping to improve our understanding of OME chemistry.

This new work extends capabilities of DLR Concise [48,49] with addition of oxygenated fuel species. DLR Concise is intended as a single flexible reaction model for alternative fuel surrogates; its target application remains both aviation as well as transportation fuel surrogates. In this context the previous DLR Concise version [48,49] is extended in this work to also now include additional components relevant solely to transportation fuel. Exploring low-temperature chemistry of transportation fuels is crucial as internal combustion engines are often affected by autoignition behavior at low-temperature regimes. For practical reasons, we include low-temperature chemistry of OME0 to OME5 as well as of n-heptane and iso-octane to describe primary reference fuel (PRF). Additionally, reactions related to predictions of NO_x chemistry are included from [50].

In this work, we present a detailed description alongside an extensive validation of OME_x (x = 0–5) chemistry and discuss various aspects of its reaction kinetics such as its global reactivity and influence of OME chain-length on its reactivity. OMEs are also attractive blending components and its ignition promoting effect on hydrocarbons is investigated. NO emissions are important aspects of transportation fuels, and chemical interactions of NO_x chemistry with hydrocarbons are known. The influence of NO_x chemistry on OME reaction kinetics is also presented. Given the extensive literature on neat OMEs, alcohols, diesel, gasoline, their mixtures, as well as on NO_x and soot related topics, this work will only discuss selected studies.

To enhance the study on OMEs and extend the DLR Concise capabilities for oxygenated fuels, new experimental data for alcohols (methanol, ethanol, n-butanol) and PRF90 measured in DLR's high-temperature flow reactor are appended. Measurements of up to 40 species mole fraction profiles of various fuel products and intermediates are identified and calibrated, complementing our extensive experimental database on hydrocarbons, oxygenates and jet fuels [48,49,51–54].

1.1. Applicability of OMEs to modern diesel engines

Several engine studies have demonstrated reduction in soot emission when using neat or blended OMEs over conventional fuels [55–58]. As Table 1 shows, the physical properties of OMEs are similar to diesel [55]. An overview of physicochemical properties of OMEs and diesel can be found in [8,32]. The ignition properties of OMEs are suitable, with their cetane number (except OME1 with 29) well above 51, a standard EN590 regulations of European diesel [8]. Investigations show that neat or blended diesel/OMEs significantly reduce soot and NO_x emission through exhaust gas recirculation (EGR) [56,59–61]. Replacing C-C bonds with C-O bonds alters their physical properties, resulting in higher density, boiling and melting points [8] (see Table 1).

Therefore, not all OMEs comply with standard diesel requirements, limiting their use as blends with diesel or requiring engine modifications [61,62]. Various concepts for better operability range of neat OMEs through modification of injector nozzle or on engine design are investigated [60,61]. Through such modifications, OMEs provide definite chance for reduced particulate and NO_x emissions.

The DLR Concise allows modeling various combination of OME mixtures with hydrocarbons for investigation of combustion and emission characteristics. Combined with physicochemical properties, this can help to explore suitable blends for engine applications.

2. Experimental data for validation

In this work, comprehensive in-house experimental data published earlier are available for the mechanism validation. These includes ignition delay times [33,63], species measurements at pyrolysis and oxidation condition in shock tubes [64], laminar flame speed obtained from laminar premixed flames [65], species profiles measured in high-temperature flow reactor [35] and in low-pressure premixed flames [34]. For details of the respective experimental setups and conditions we refer to the original literature. Additionally, new measurements of C_1, C_2 and C_4-linear alcohols as well as PRF90 obtained in the DLR flow reactor are presented in this work. A brief summary of available experimental data is given in Table 2.

A large body of experimental work available in literature, mostly for OME0 to OME3, is also used for the model validation. A brief summary is given in **Table S1-S5** in supplemental material: more than 200 datasets from five different experimental setups covers combustion conditions of $T = 500–2000$ K, $p = 0.03–55$ bar and fuel stoichiometry of $\Phi = 0.2–2.0$.

3. DLR Concise – Model description and validation

DLR Concise is a semi-detailed high-temperature reaction model which, through lumping isomers, restricts the mechanism to a minimum number of species but is still capable of predicting detailed chemistry. This enables to incorporate large number of fuel surrogate components in a single mechanism for simulating wide variety of surrogate fuels irrespective of its application. This allows DLR Concise for resolving the impact of the chemical composition of complex technical fuels on reaction performance and pollutant formation [49,67].

Table 1
Properties of OMEs and diesel, data source [8,32].

	OME_0	OME_1	OME_2	OME_3	OME_4	OME_5	OME_6	OME_7	Diesel EN590
chemical formula	$C_2H_6O_1$	$C_3H_8O_2$	$C_4H_{10}O_3$	$C_5H_{12}O_4$	$C_6H_{14}O_5$	$C_7H_{16}O_6$	$C_8H_{18}O_7$	$C_9H_{20}O_8$	C_{12}-C_{20}
molecular weight	46	76	106	136	166	196	226	256	109–202
H/C	3	2.67	2.5	2.4	2.33	2.29	2.25	2.22	~1.952
O/C	0.5	0.67	0.75	0.8	0.83	0.86	0.88	0.89	0
cetane no.	55	29	63	78	90	100	104		>51
octane no.		77	48						
%oxygen	34.8	42.1	45.3	47.1	48.2	49	49.6	50	0
density @25°C (g/cm^3)	0.67	0.86	0.96	1.02	1.06	1.1	1.13	1.16	0.82
density @40°C (g/cm^3)		0.318	0.559	0.86	1.32	1.93			2.5–3.2
melting point (°C)	-138	−105	−65	−41	−7	18.5	58		−15 to 5
boiling point (°C)	-25	42	105	156	202	242	280		160–338
LHV (MJ/kg)	28.8	22.44	20.32	19.14	18.38	17.86	17.47		25
kinematic viscosity @25°C (mm^2/s)	0.184	0.36	1.08	1.72	2.63				2–4.5
surface tension (mN/m)		20.4	28.8	30.7	32.6				

Table 2
List of in-house experimental data used for validation.

Fuel	Setup	Property	Conditions	T(K), p(bar)	Ref.
OME0-2, OME4, OME1+PRF90, PRF90	Shock tube	IDT	$\Phi = 1.0$ fuel-synthetic air dilution 1:5 with N_2	950–2000 K; 1, 4, 16 bar	[33,63,66]
OME0-2	Single pulse shock tube	SP	$\Phi = 0.5, 1.0, 2.0, \infty$ $\geq$ 99.45% Ar/Xe	900–1550 K; 16 bar	[64]
OME1-2, OME4, OME1+PRF90, OME4+Diesel surrogate	Bunsen type burner	LFS	$\Phi = 0.6$-2.0 pressurized air	$T_{preheat}$ = 473 K; 1, 3, 6 bar	[33,63,65]
OME0-5, CH_3OH*, C_2H_5OH*, n-C_4H_9OH*, PRF90*	High-T flow reactor	SP	$\Phi = 0.8, 1.2, 2.0^{\#}$ Fuel/O_2/(9.9slm)Ar ($^{\#}$1.5 for alcohol)	1 bar	[35] *Present work
OME0-3	Flat-Flame burner (McKenna)	SP	$\Phi = 1.7$ Fuel/O_2/(50%)Ar	0.04 bar	[34]

IDT: Ignition delay times, LFS: Laminar flame speed, SP: speciation.

In this work, DLRConcise2021v1.JF [48] is modified and extended to (1) improve minor open problems, for example, separating C_3H_4, C_3H_5 and C_4H_8 isomers for enhancement in iso-octane chemistry, (2) include high- and low-temperature OME chemistry, (3) include low-temperature PRF components n-heptane and iso-octane chemistry, and (4) append with the Glarborg NO_x mechanism [50] for the prediction of NO_x emissions. The presented, DLRConcise2024v2.F (Fig. 1), extends jet fuels to transportation fuels with capability of predicting OMEs and hydrocarbons chemistry along with NO_x as well as soot precursors emissions. This includes among the cyclic hydrocarbons, cyclo-paraffins such as cyclohexane, n-propylcyclohexane, decalin, mono-aromatics such as benzene, toluene, propylbenzene, styrene, as well as multi-cyclic-aromatics such as indane, indene, tetralin, naphthalene, methyl-naphthalene, biphenyl, phenanthrene, pyrene as well as larger aromatics up to C20 [48]. This DLR Concise contains 318 species and 2208 reactions for the description of high-temperature chemistry. Additionally, 152 species and 338 reactions are included for an optional low-temperature chemistry module and 81 species and 795 reactions for the description of NO_x chemistry from [50] including additional 6 reactions inserted for each OME-NO sensitization discussed later in Sec. 4.4.

For the reaction kinetics, the determination of the reaction rates is as important as the feasibility estimation of the reaction. The linear OME molecules contain two types of bonds on primary (p) and secondary (s) carbon atoms namely, p(C-O), s(C-O), p(C-H), s(C-H). The terminal p(C-O) bond in OMEs is the weakest compared to s(C-O) bond, which is in contrast to equivalent alkane where the p(C-H) bond at primary carbon position are the strongest [8]. As presented in Fig. 2, the bond dissociation energies of p(C-O), s(C-O), p(C-H), s(C-H) of OME$\geq$1 are similar [27,44], which allows to consider reaction rates of OME >1 from analogy of OME1.

The BDEs of the bonds involved in the structure of OMEs to equivalent alkanes or ethers differ. This disapproves to draw analogies from them to estimate reaction rates often applied in hydrocarbons [8]. Except few reactions of OME2 [69], the reaction rates of OME_x with x>1 are not investigated directly and the reaction mechanisms rely on rate rules-based estimations or use of analogy from DME and OME1. The reaction mechanism of OMEs presented in this work includes

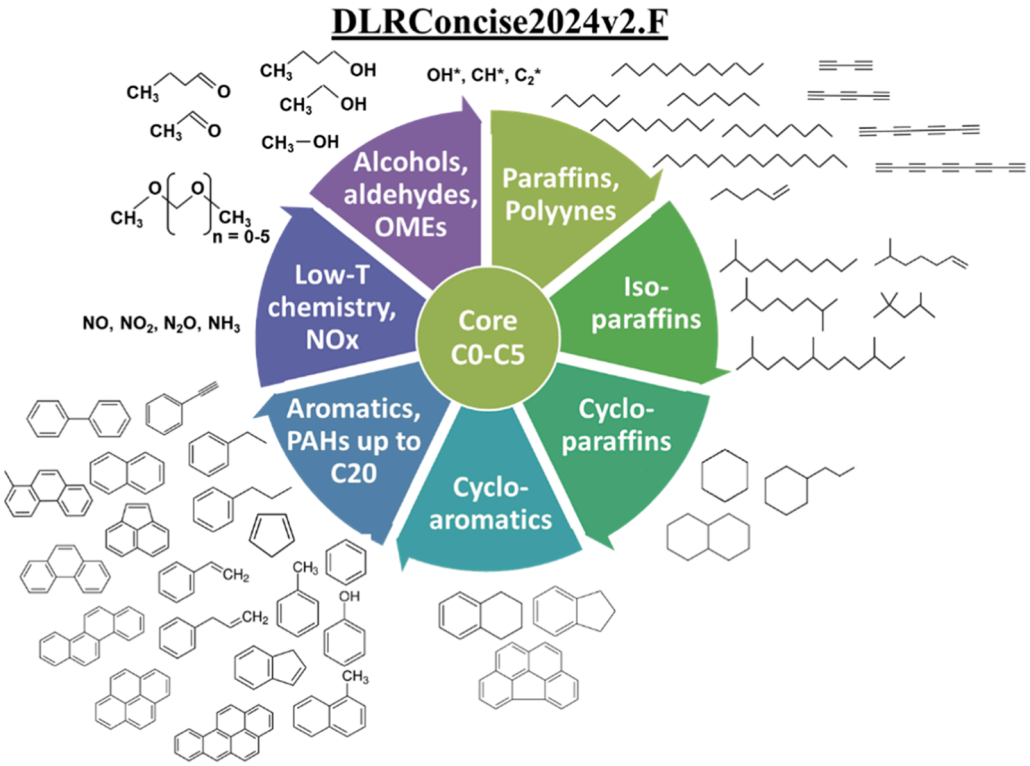

Fig. 1. Schematic of DLR Concise.

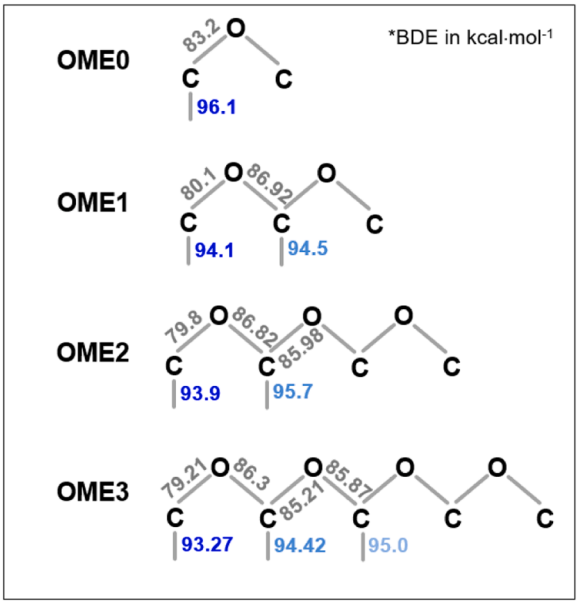

Fig. 2. Bond dissociation energies (BDEs) of OME0-3 at 0 K [68,27].

well-established reaction classes and the thermochemical and transport properties data are taken from diverse literature sources and are cited in the corresponding data files.

3.1. Oxymethylene ethers (OMEs)

The chemistry of dimethyl ether, the smallest among OMEs (x = 0), is also important for the complete description of larger OMEs. The major thermal decomposition route in the high-temperature regime of DME generates CH_3 and CH_3O radicals while undergoing a C-O bond cleavage. A pressure-dependent rate coefficient, estimated through combination of shock tube measurement and *ab initio* calculations, is adapted from Sivaramakrishnan et al. [70]. The typical H-atom abstraction from DME molecule (with X = O, H, OH, CH_3, CH_3O, HO_2, O_2) produces methoxy methyl radicals (CH_3OCH_2 = DME*-1). The decomposition of CH_3OCH_2 gives formaldehyde and methyl radical. The sources of their reaction rates and the pressure-dependent rate coefficients of reactions describing low-temperature chemistry are mainly adopted from Burke et al. [16]. Additionally, the self-reaction of DME*-1OO (RO_2 radical) and its decomposition by losing OH radical [24] are incorporated, forming methyl formate (CH_3OCHO) at low temperatures. Also, reactions involving consumption of methyl formate and formic acid are included.

The reaction pathways of DME oxidation are presented in Fig. 3 for ignition conditions. At all temperatures, the production of DME*-1 in the H-atom abstraction reactions is mainly by OH radicals. Second important route is the ß-scission of DME*-1 forming CH_3 radical and formaldehyde which is the main DME consumption route leading to formation of CO and CO_2 via formaldehyde. The methyl recombination route is leading to C_2 chemistry (at high T). With the decrease in temperature, the molecular oxygen addition to the fuel radical (DME*-1) leads to the formation of methoxymethyl-peroxy radical (DME*-1OO), which can undergo intramolecular isomerization to form the QOOH: hydroperoxymethoxymethyl radical (DME-1OOH-3*). At temperatures below 600 K, a second O_2-addition to DME-1OOH-3* leads to the formation of peroxymethoxymethyl-hydroperoxide radical (DME*-1OOH-3OO) which decomposes to ketone releasing two hydroxyl radicals in two reaction steps. Thus, the formation of hydroperoxyl-methyl formate (DME-KET13) and the two hydroxyl radicals increases the reactivity. At intermediate temperatures (>600 K), ß-scission of DME-1OOH-3* radical forms hydroxyl radical and two formaldehyde molecules thereby giving

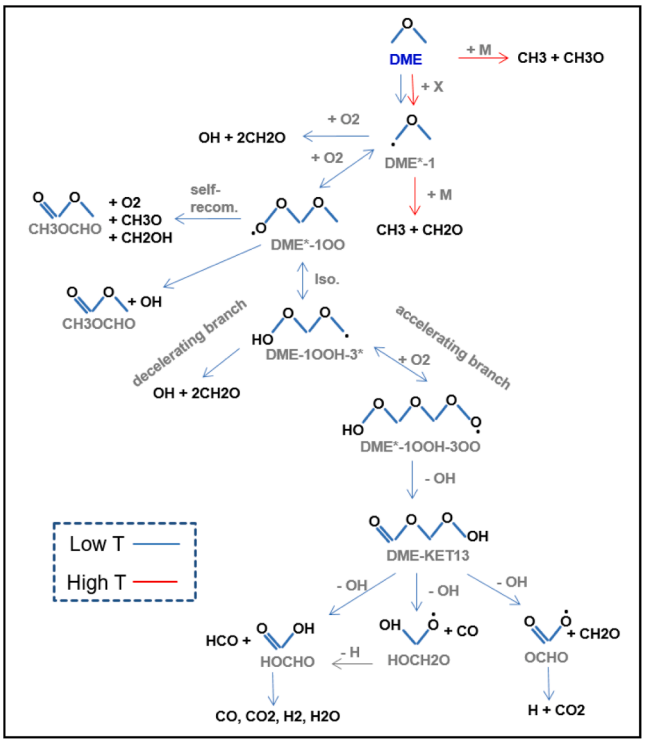

Fig. 3. High- to low-temperature reaction routes of DME included in the DLR Concise.

negative temperature dependence before the high-temperature chemistry overtakes to increased reactivity. Also, the methyl radicals formed can activate low-temperature methyl radical chemistry leading to the formation of methyl-peroxy and methyl-hydroperoxide chemistry. These reaction routes are widely studied and accepted in literature [71, 16,68].

The Fig. 4 shows general depiction of OME1 conversion in the mechanism for entire temperature range. At high temperatures, the decomposition of the OME1 occurs via three major reactions (R1)-(R3). The roaming reaction giving methanol and a carbene (R4), suggested in [21,25,72], is sensitive to the selection of H-atom abstraction rate of OME1 with CH_3 and subsequently influences the amount of methanol formed (see **Fig. S2.6** in supplemental material).

$$\text{OME1 (+M)} = \text{COCO*} + \text{CH}_3\text{ (+M)} \quad \text{(R1)}$$

$$\text{OME1 (+M)} = \text{DME} + \text{CH}_2\text{O (+M)} \quad \text{(R2)}$$

$$\text{OME1} = \text{DME*-1} + \text{CH}_3\text{O} \quad \text{(R3)}$$

$$\text{OME1} = \text{CH}_3\text{OH} + \text{CH}_3 + \text{HCO} \quad \text{(R4)}$$

The rate of reaction (R1) is based on the thermal dissociation of dimethyl ether from Sivaramakrishnan et al. [70]. The rate coefficients for (R2) to (R4) are from Yasunaga et al. [73]. The above rate coefficients are directly adopted from the stated source. In addition to (R4), methyl radicals are directly formed via C-O bond cleavage from the fuel radicals in reaction,

$$\text{OME1*-3} = \text{CH}_3\text{OCHO} + \text{CH}_3 \quad \text{(R5)}$$

and indirectly from reaction (R6) where DME*-1 radical decomposes to give CH_3 and CH_2O,

$$\text{OME1*-1} = \text{DME*-1} + \text{CH}_2\text{O} \quad \text{(R6)}$$

Thereby the reactions forming and consuming CH_3 radicals are important to the OME1 conversion.

In the H-atom abstraction reactions from OME1, depending on

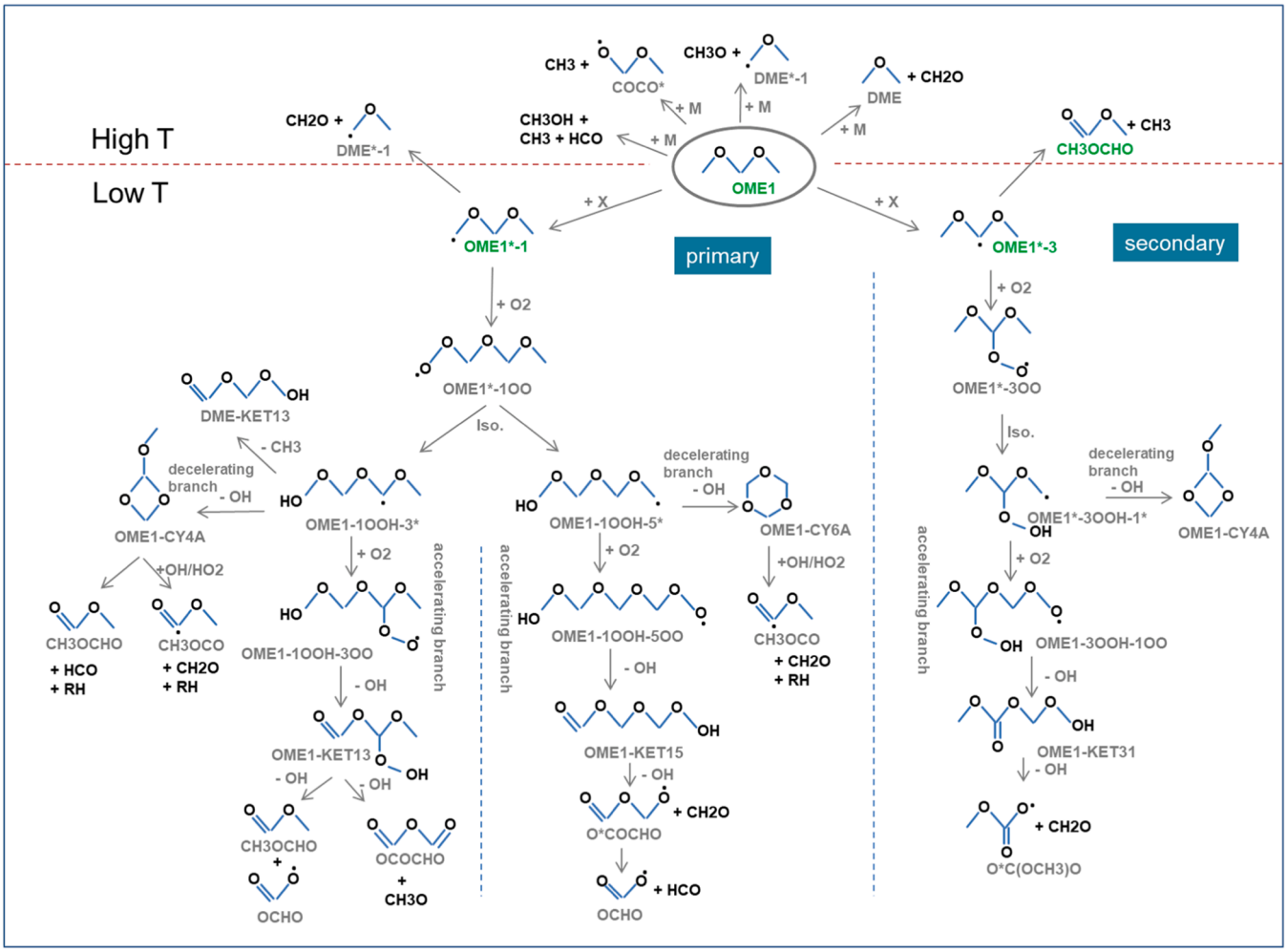

Fig. 4. High- to low-temperature reaction routes of OME1 included in the DLR Concise.

temperature, the main H-atom abstraction partners are OH, H, CH_3, CH_3O, O_2, and HO_2. Among them, the major influence of H-atom abstraction is by OH, H, and CH_3, a relative importance among them varies by different reaction mechanisms. In DLR Concise, the formation route of the primary fuel radical OME1*-1 by H-atom abstraction is marginally preferential than the secondary radical OME1*-3 at high temperatures. This is in accordance with most of the literature mechanisms [24,25,28,31,32,40]. The mechanism from [27] is an exception and is predominant on the primary carbon site. In the region of the negative temperature coefficient (NTC) and at low temperatures, both channels are nearly equal. A rate of production analysis supporting this is available in **Fig. S2.4** in the supplemental material.

At high temperatures, the H-atom abstraction leading to OME1*-1 is chain propagating as it subsequently leads to the formation of methoxy methyl radical (DME*-1) (R6), whereas the secondary radical gives methyl formate (CH_3OCHO) through methyl radical elimination (R5). Equally during pyrolysis, the primary and secondary fuel radicals stay important whereas unimolecular fuel decomposition reaction accounts for <10% contribution at both pyrolysis and oxidation conditions. The branching ratio between the primary and secondary radical formation is not consistent among the literature mechanisms and the differences in selectivity towards primary or secondary radicals is discussed in Fernard & Vanhove [8]. However, the deviations among the various predicted combustion parameters are within the acceptability range (see comparison of literature mechanisms in **Figs. S61-S62** in supplemental material).

With the decrease in temperature, the reactivity of OME1 in the NTC region is mainly dominated by O_2 addition to primary (OME1*-1) as well as secondary (OME1*-3) radical, which also becomes important at low temperatures. The formation of methyl formate from secondary fuel radical (R5) persists even at low temperatures (due to their low energy barrier) which is also evident from the reactor measurements (**Figs. S34, S48** in supplemental material). As a result of O_2 addition, two corresponding peroxy radicals OME1*-1OO ($CH_3OCH_2OCH_2OO$) and OME1*-3OO ($CH_3OCH(OO)OCH_3$) are formed (Fig. 4). The energetic stable QOOH radicals are formed from peroxy radicals via intramolecular hydrogen transfer. From RO_2 to QOOH, the intramolecular H-transfer between two carbon sites are considered for maximum 8-membered ring transition states. As shown in Fig. 5, in case of primary radicals 6- and 8-ring transition occurs whereas for secondary radical only 6-ring transition takes place (ring transition for other OMEs are presented in **Fig. S107** in Supplemental material). The consumption of QOOH occurs via ß-scission forming ketone DME-KET13 or to cyclic ethers OME1-CY4A (methoxy-1,3-dioxetane), and OME1-CY6A (1,3,5-trioxane) by releasing hydroxyl radical. The formation of cyclic ethers has inhibiting effect on the global reactivity of the OME molecule. With further decrease in temperature, second addition of O_2 to QOOH leads to the formation of O_2QOOH which rapidly dissociates to give a keto-hydroperoxide (KHP) and a carbonyl-hydroperoxide (CHP), by releasing hydroxyl radicals. The reaction rates of low-temperature OME1 chemistry are mainly from Jacobs et al. [25].

Due to their chemical similarity and absence of direct evidence, the reaction rates involved in the description of OME2 to OME5 reactions in DLR Concise are based on the analogy of OME1. A detailed description

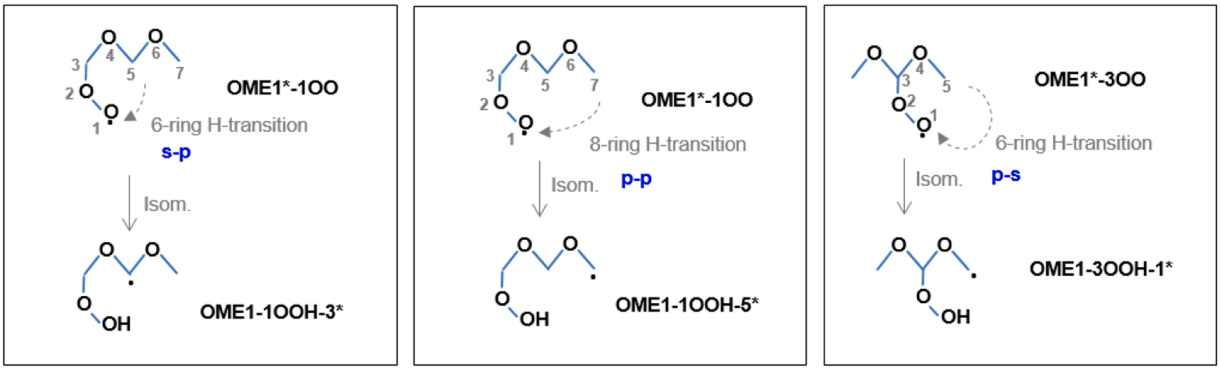

Fig. 5. Intramolecular H-transfer in OME1 during isomerization reaction of RO_2 to QOOH.

of reaction routes for both low- and high-temperature reactions included in the reaction mechanism of OME2-5 is similar to the one discussed in OME1 and are presented in the supplemental material (**Sec. S4**).

3.1.1. Ignition delay times

The model predictions of ignition delay times (IDT) of OME0-4 measured in shock tubes are available for diverse combustion conditions [16,74,19,31,63]. Fig. 6 shows that the IDTs of DME are excellently reproduced for fuel-lean to fuel-rich stoichiometries and at wide temperatures including NTC.

The IDTs of OME1 (Fig. 6**)** are measured at fuel stoichiometries of 0.5–2.0 and pressures from 1–9 atm. The IDTs increase with stoichiometry at atmospheric pressure and high temperatures as seen in **Fig. 6 (1)**. However, with decrease in temperature and increase in pressure as shown in **Fig. 6(2)**, the stoichiometric differences narrow down at high temperatures and further in the NTC and at low temperatures there is an inversion in the ignition behavior. At intermediate temperatures, the OME1 shows a slightly reduced reactivity but no prominent NTC behavior. The effect of dilution can be observed in **Fig. 6(3)** where for a given stoichiometry and pressure, the decrease in dilution ratio of Ar/O_2 (or increase in fuel concentration) causes – as expected – increased reactivity. The model is capable of accurately predicting the measured behavior. The modeled IDTs of OME2-5 reproduce the measured weak reactivity in the NTC region well, though they over-predict measured IDTs around the NTC for OME2 and OME3. Additionally, in absence of IDTs of OME5 and due to similar reactivity of higher OMEs, the measured IDTs of OME4 [31] are compared with modeled OME5 data which are in good agreement. IDT comparisons from [63] are available as supplemental material in **Figs. S1-S10**.

3.1.2. Laminar flame speeds

Among the global combustion parameters, the laminar flame speeds and burning velocities of OME0-4 are presented in Fig. 7. The burning velocities [75,77] and flame speeds of DME [76,26] at various pressures [75,76,26] and at various preheat temperatures [77] are well reproduced by the mechanism at all fuel stoichiometries. Unlike hydrocarbons, the maximum flame speeds of OMEs are at slightly richer stoichiometries (Φ =1.2 instead of 1.1). The laminar flame speeds of OME1 are measured in several studies [26,32,33] at various preheat temperatures as shown in Fig. 7. With increase in preheat temperatures, the flame velocity increases. The model well reproduces the flame velocities at given conditions, though the measurements of [33] tend to peak at slightly higher stoichiometry. The laminar flame speeds of OME2 as a function of fuel stoichiometry, preheat temperature and operating pressure are excellently reproduced by the DLR Concise. The burning velocities [27,78] and flame speeds [32] of OME3 are obtained for various fuel stoichiometries where both temperature as well as pressure dependence (**Fig. S21** in supplemental material) are reproduced by the model for lean to rich conditions. For OME4 [65], the flame speeds are considerably under-predicted by the model at all preheat temperatures and pressures (also by Cai model [31], **Fig. S74** in Supplemental material). Although, similar flame speeds are expected for OME $\geq$2 (also similar reactivity observed in [44,40,31,32,35,34]), measured flame speeds of OME4 [65] are significantly higher compared to the values of OME2 (up to 8% higher at $\sim \Phi = 1.1$ and even more at higher stoichiometries). Presently, DLR Concise and [31] are the only available reaction models where the latter has not been specifically examined for flame conditions, further investigations of flame speeds in the future, may clarify the discrepancies between the experimental and modeling results.

3.1.3. Speciation in flow reactors

Low temperature oxidation of DME was measured in jet-stirred reactor (JSR) [38,68,79] and in flow reactor [39]. As shown in Fig. 8, the fuel conversion shows decreased reactivity between 500–600 K, also reflected by the model. Key products of DME low-temperature chemistry were measured and quantified with measurement uncertainties as high as factor of 4 [79,39]. The modeled DME-KET13 peaks at early temperatures whereas formic acid is well reproduced by the model. In addition, methyl hydroperoxide (CH_3O_2H), formaldehyde, methyl formate and hydrogen peroxide are also quantified [79,68]. As discussed earlier, the formation of formic acid is from DME-KET13 decomposition whereas the formation of methyl formate is a result of self-recombination or decomposition of methoxymethyl-peroxy radical. At low temperatures, CH_3O_2H is formed from O_2 addition to CH_3 radical and subsequent reaction of methoxy radical to methyl-hydroperoxide. The source of the CH_3 radical is either decomposition of CH_3OCHO or CH_3OCH_2 radical (see **Figs. S45-S46** in Supplemental material for additional plots).

Measurements of OME1 in JSR, performed by Vermeire et al. [24] and Sun et al. [23] are shown in Fig. 8. The experiments from [24] are available at both pyrolysis (**Fig. S49**, supplemental material) and oxidation conditions. The oxidation data shows slight reduction in reactivity in intermediate temperatures. The formation of methoxy-1, 3-dioxetane (OME1-CY4A) around 550 to 800 K is over-predicted by the model by a factor of three. High-pressure oxidation of OME1 [23] at 10 atm shows good agreement of modeling predictions of major C_1-C_2 hydrocarbons and oxygenated intermediates.

In Fig. 8, OME2 oxidation in JSR [44] was measured for temperatures ranging from 500 to 1000 K for three fuel stoichiometries. The species profiles of major species show slightly reduced reactivity in the temperature around 600 K, similar to the observed behavior in ignition delay time measurements by Cai et al. [31]. Additional validation is available in the supplemental material (**Fig. S51**). The only oxygenated intermediate species measured in this work are methyl formate (CH_3OCHO) and methoxy-methyl formate (COCOCHO) which are formed at both high and low temperatures. The COCOCHO is well predicted at all temperatures, whereas methyl formate at low temperature

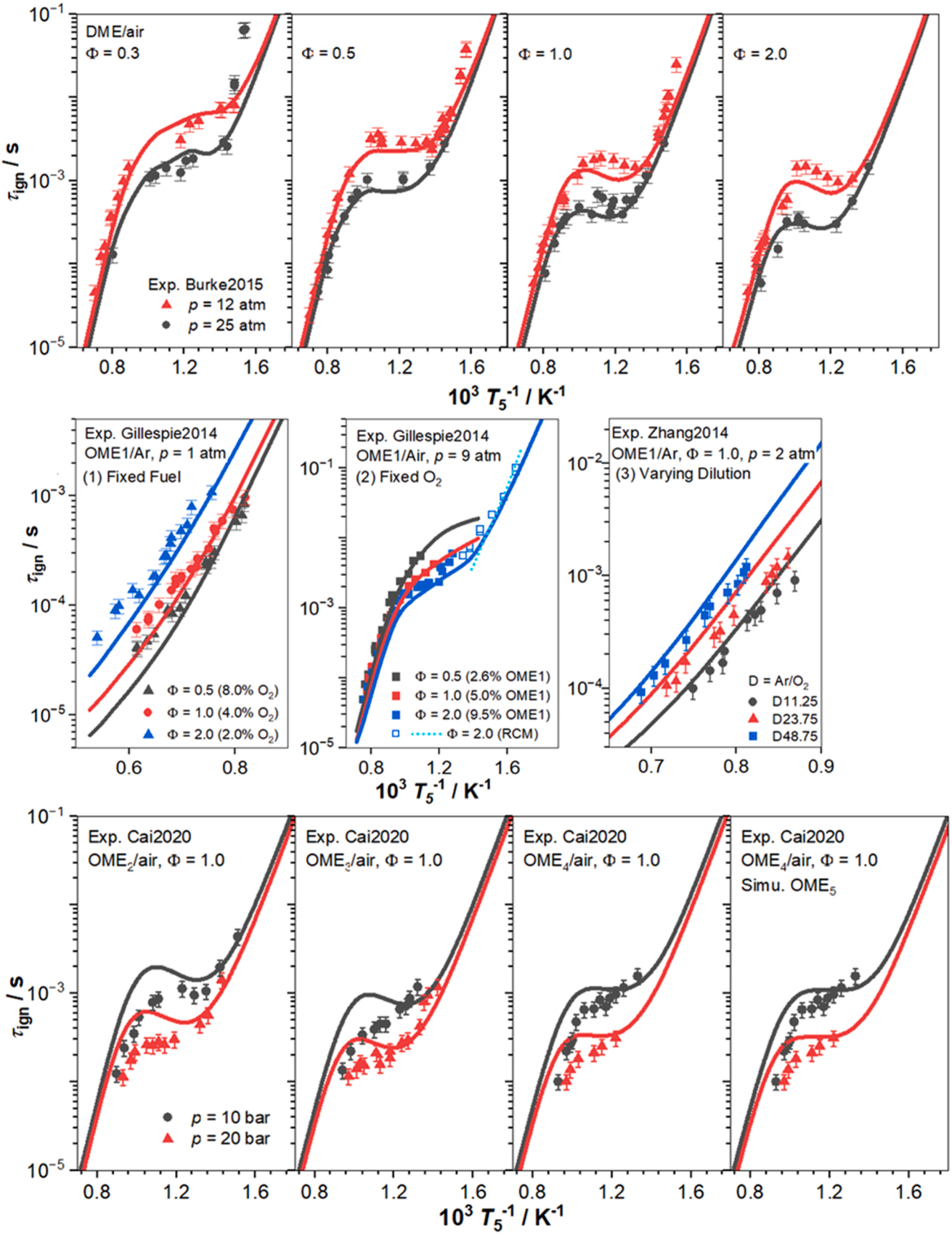

Fig. 6. Comparison of measured (symbols) and modeled (curves) ignition delay times measured in shock tubes: DME [16], OME1 [74,19], and OME2-5 [31].

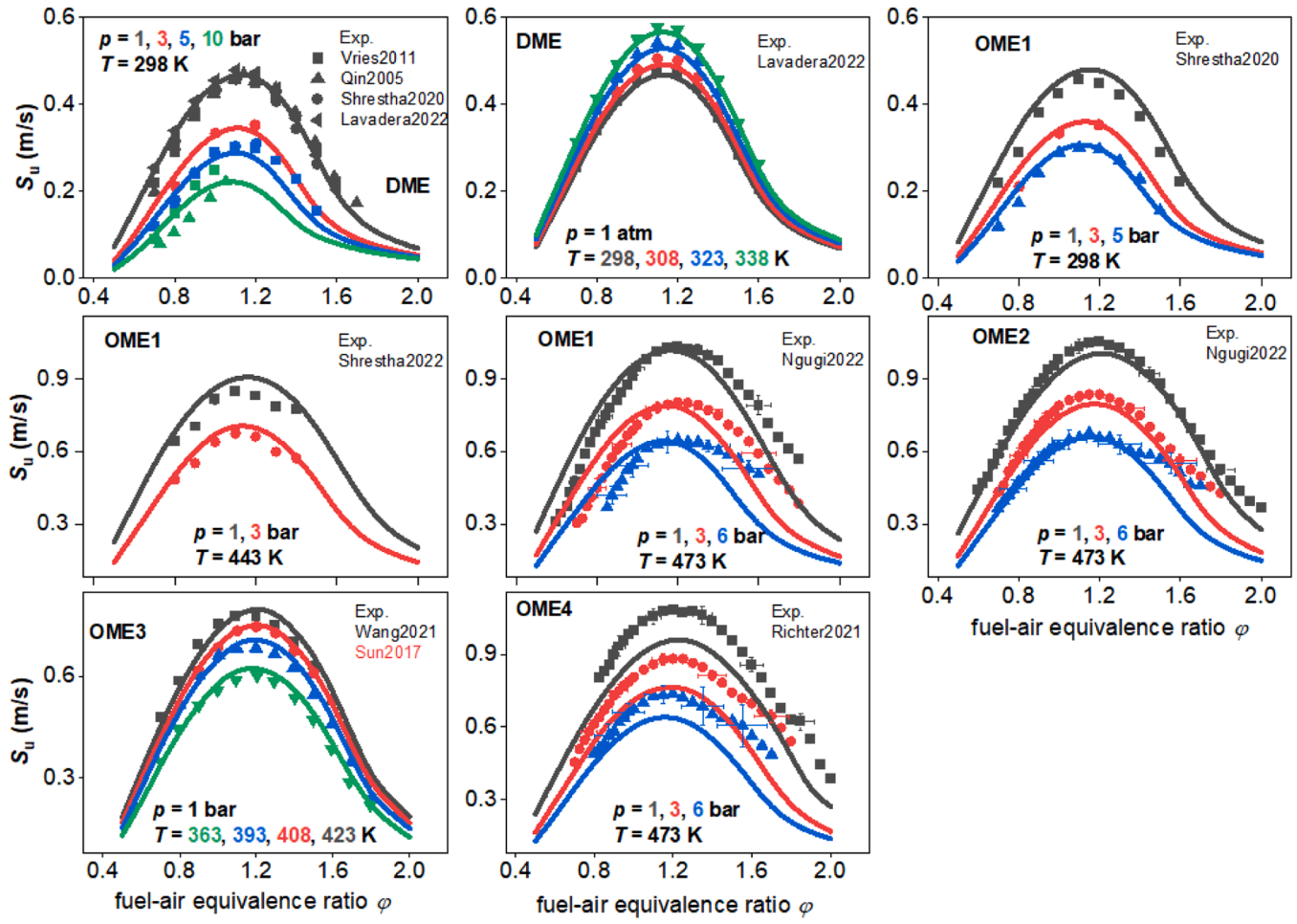

Fig. 7. Comparison of measured flame speeds or burning velocities (symbols) and modeled flame speeds (curves) of DME [26,75,76,77], OME1 [32,33], OME2 [66], OME3 [27,78], OME4 [65].

is within uncertainty range of measurements but is underpredicted at higher temperatures. The main formation route of both of them is through secondary fuel radical (OME2*-3) decomposition, thus their temperature dependence and branching ratio are important. The prediction of methyl formate and methoxy-methyl formate varies among literature mechanisms, see **Fig. S92** (in supplemental material). This is likely due to slight variation among the branching ratio of OME2 to primary and secondary radical whereas the direct source reaction of methyl formate (*s*-OME2=$CH_3OCHO+CH_3OCH_2$) shows less sensitivity (more see **Fig. S2.7**).

The major species for the validation of OME3 low-temperature chemistry are available from the recent JSR measurements by Qiu et al. [42]. As shown in Fig. 8, the model is capable of reproducing excellently the OME3 and oxidizer conversion to major product formations in temperatures ranging from 500 K to 1000 K.

Recently, OME2 oxidation was measured in a burner-stabilized cool flame [80]. Among other oxygenates, they measured methoxy-methyl formate around 400–900 K (Fig. 9). Similarly, COCOCHO is also measured in OME3 oxidation in a JSR [44] around 500–900 K, no measurements are reported at higher temperatures. Also, literature mechanisms predict COCOCHO in OME3 [44] (**Fig. S93**, supplemental material). To our knowledge, none of the other existing measurements have shown experimental evidence of methoxy-methyl formate in measureable amount. In a OME3 flame, no detection of COCOCHO and COCOCOCHO is reported in [27] where possible fast dissociation is assumed. Considering high flame temperatures in [27] compared to low temperatures of [44], the fast decomposition of COCOCHO seems a feasible explanation. The simulations of OME3 flames [27] with all the available OME3 reaction models [31,32,27] – including present work – however predict COCOCHO within 2000–5000 ppm range. At current state, the stability and temperature dependence of COCOCHO is unclear and more experimental proof is required for a detailed understanding, which may also lead to changes in the reaction models.

Compared to OME0-3, for OME4-5 only our in-house speciation data measured in a flow reactor [35] are available. Fig. 10 shows model predictions of both fuels and oxidizer conversion of OME4 and OME5. Among major species, CH_4 and C_2H_4 are well predicted by the model. The formation of soot precursor C_2H_2 was below the detection limit [35], also confirmed by the model. For both cases, the oxygenated product CH_2O is over-predicted by the model by a factor of two compared to the measurements, CH_2CO and methyl formate are predicted within the uncertainty limits of measurements (20%).

3.1.4. *Speciation in laminar flames*

For the prediction of high-temperature flame chemistry, measurements of OME0-OME3 in burner-stabilized flames are shown in Fig. 11. The fuel and oxidizer conversion and major product formation of fuel-rich DME flames [81] are accurately predicted by the model. The radical species (O-, H-atoms, OH and HCO radicals) – rarely obtained experimentally [45] – are very well reproduced by the mechanism, which are important part of the combustion chemistry. More hydrocarbon intermediates and fuel specific oxygenates can be found in the supplemental material (**Fig. S27**).

For the OME1 premixed flames [34], the fuel and oxidizer

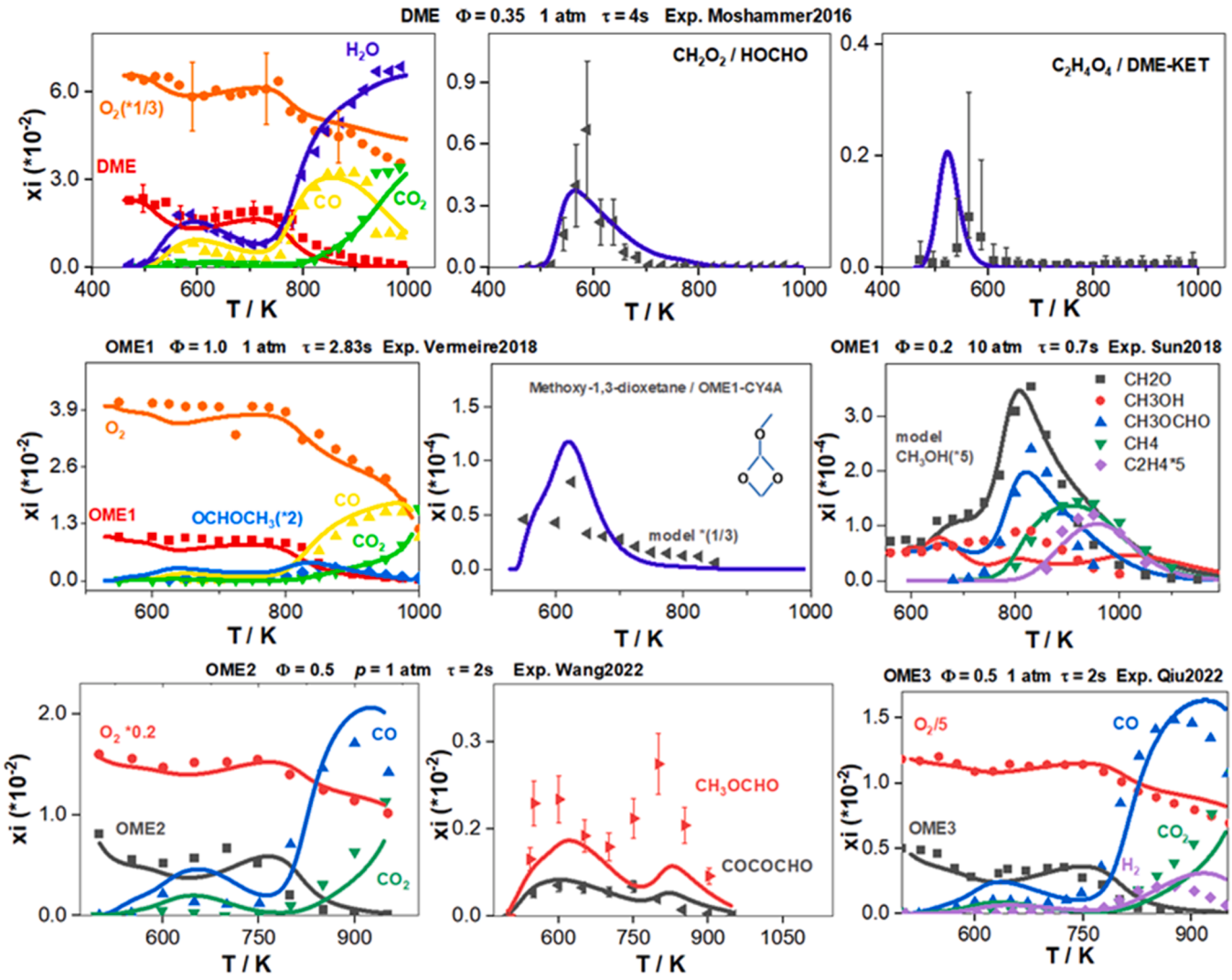

Fig. 8. Comparison of measured (symbols) and modeled (curves) OMEx oxidation in JSR. DME [79], OME1 [24,23], OME2 [44], and OME3 [42]. Scaling factor indicated when applied.

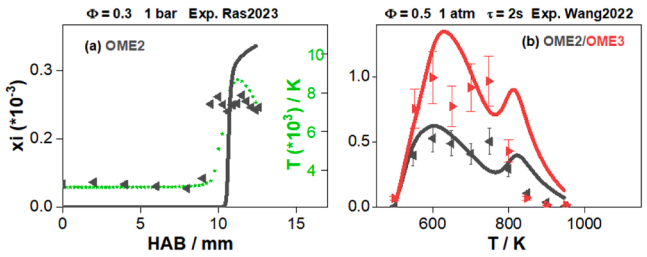

Fig. 9. Prediction of methoxy-methyl formate in OME2-3 (a) premixed cool flame on heated stagnation plate burner [80], (b) JSR [44].

consumption and main products as well as important products formation are presented in Fig. 11. Along with modeled stable C_1-C_2 intermediates, oxygenated species CH_2O, DME, methyl formate as well as formic acid are reproduced within the uncertainty limits of the measurements. Additional flame data from [22,27] at two other stoichiometries can be found in the supplemental material (**Fig. S29**). At high temperatures, the burner stabilized flames measured by Sun et al. [27] proofed significant amount of smaller OMEs. Fig. 11 shows OME0-2 formed in OME3 oxidation, where the model well predicts DME, OME1 is over-predicted whereas OME2 is underpredicted. Additionally, various oxygenated species are also measured and compared with the model.

3.2. Alcohols

To broaden the validation range on oxygenated fuels for the updated DLR Concise, we present new experimental data on C_1-C_4 alcohols measured in the DLR high-temperature flow reactor by molecular-beam mass spectrometry. Note that the experimental setup is described elsewhere [82,51,52]. The oxidation of methanol, ethanol and n-butanol are measured for three fuel stoichiometries (Φ = 0.8, 1.2, 1.5) at atmospheric pressure. Various species profiles are recorded as a function of the reactor (oven) temperature and are used for the validation of the reaction model. Detailed validation of alcohols is presented in our earlier work [48] and only comparison of modeled and measured new data are presented here. In Fig. 12, fuel and oxidizer conversion as well as main oxidation products predicted by the model are compared with the measurements. In case of methanol, both fuel and O_2 conversion is slightly faster in the model. The model reasonably predicts the measured conversion considering also the measurements uncertainty limits below 20 K shown for Φ = 1.2. For higher alcohols, ethanol and butanol presents some decrease in reactivity at mid temperatures, which is also captured by the model.

Fig. 12 shows that the soot precursor acetylene is below the measurement limit in the methanol oxidation, but increases in larger

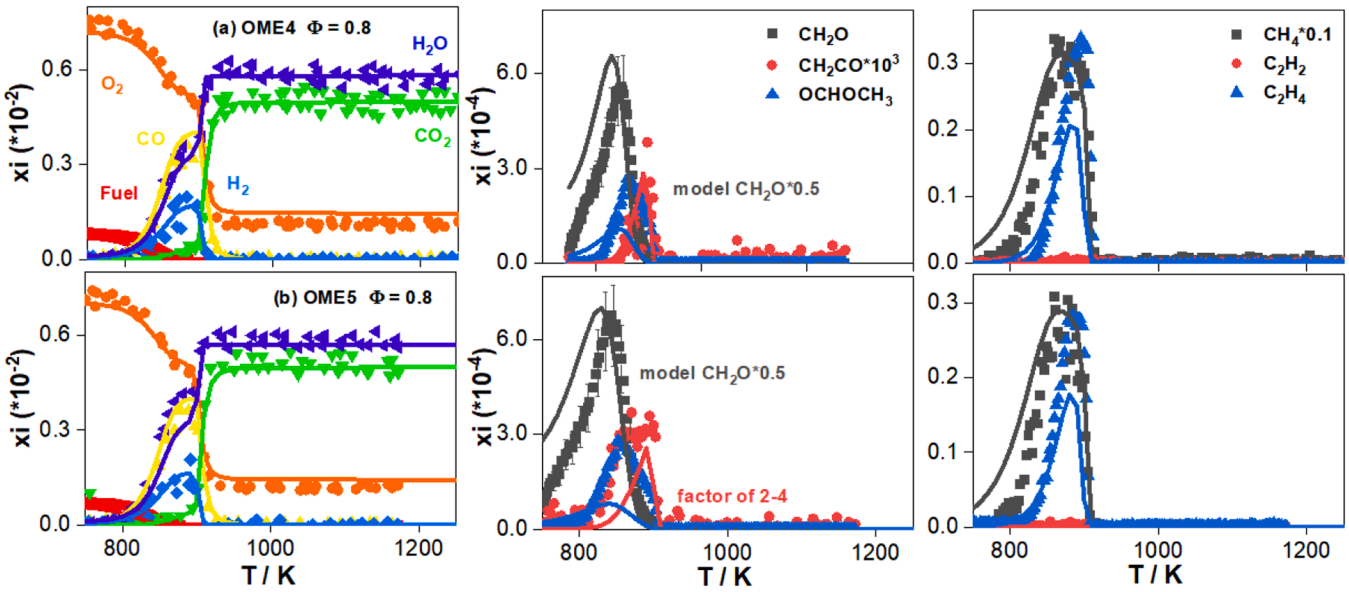

Fig. 10. Prediction of major species in DLR flow reactor [35].

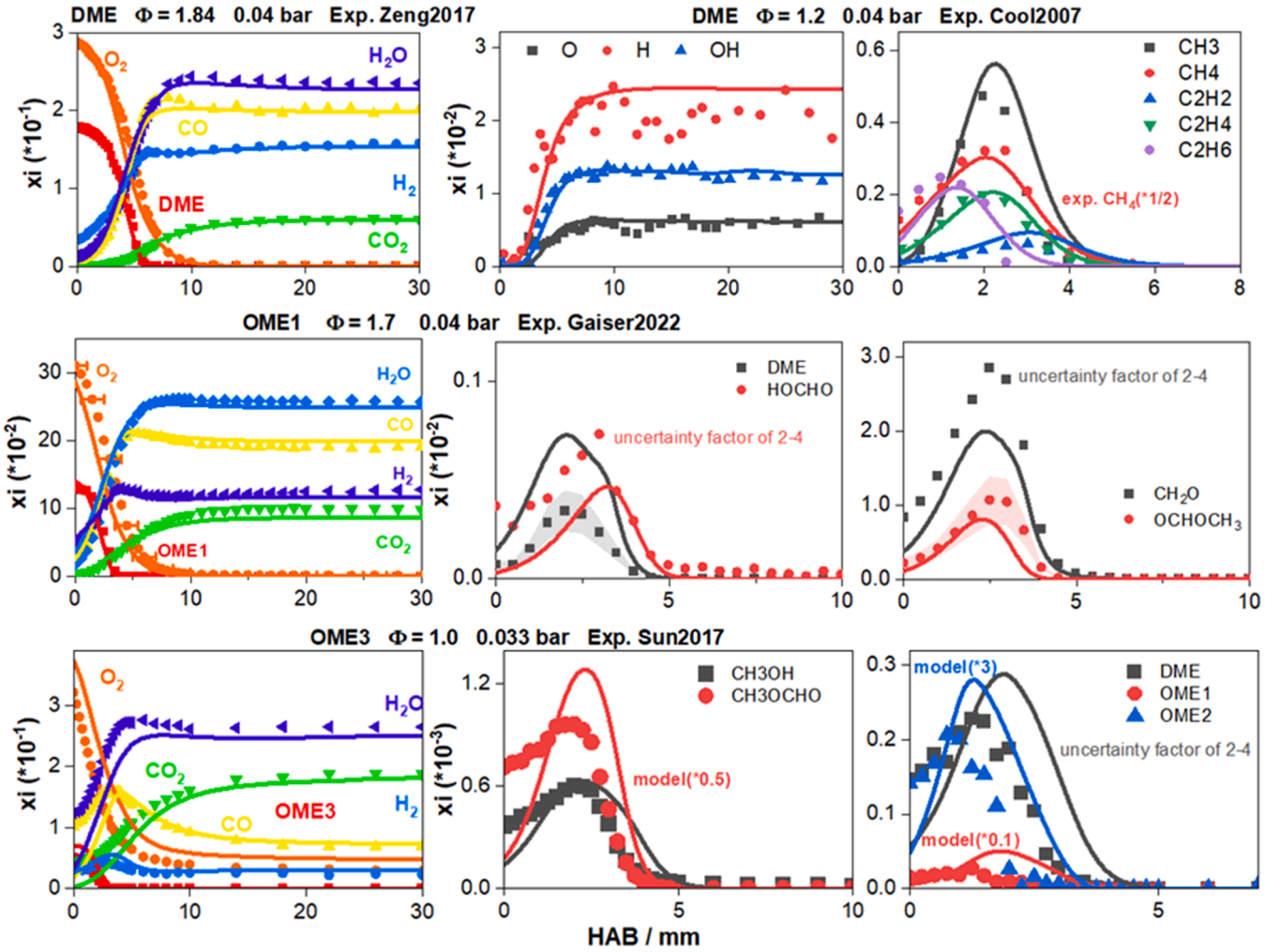

Fig. 11. Comparison of measured (symbols) and modeled (curves) species in burner-stabilized flames: DME [81,45], OME1 [34], OME3 [27]. Scaling factor indicated when applied.

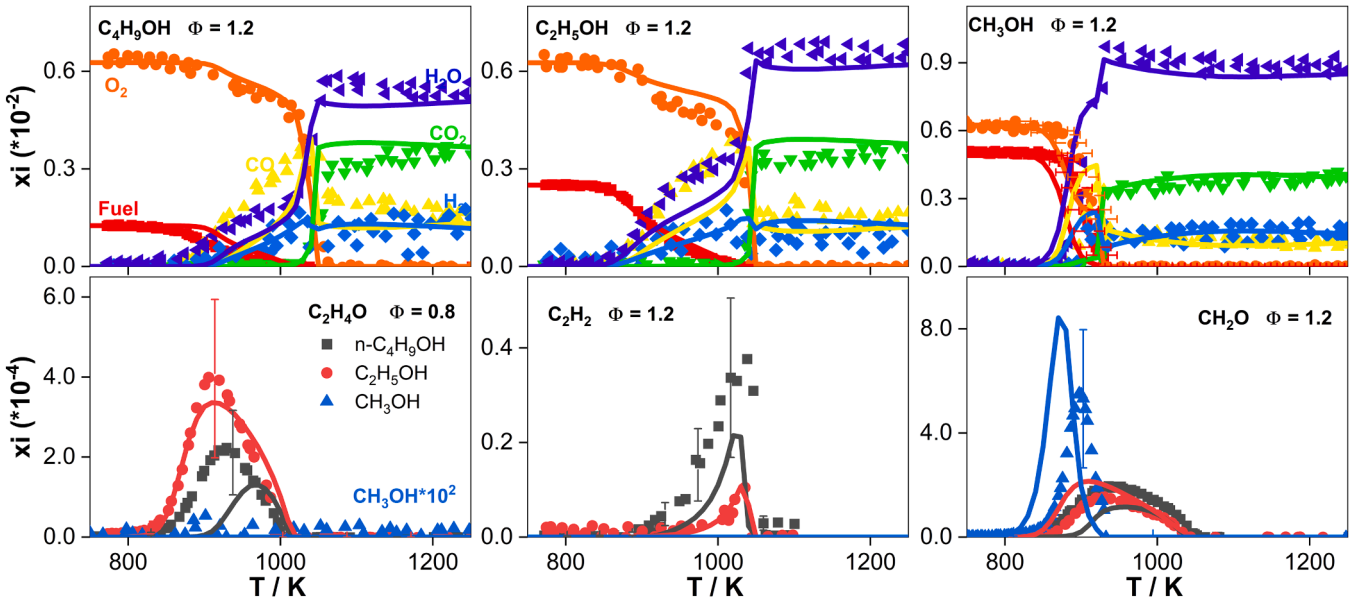

Fig. 12. Predictions of major species and important intermediates in three alcohols in DLR flow reactor.

alcohols. Note that potential oxygen containing, harmful compounds such as formaldehyde and acetaldehyde show a different trend among chain-length of alcohols. In OMEs and in alcohols, the fuel radical undergoes decomposition leading to formaldehyde and subsequently formation to CO. The formaldehyde is higher in methanol due to its direct formation through the fuel radical, whereas in ethanol and butanol the branching to secondary fuel radical decreases its concentration compared to methanol and there is small increase with increase in fuel C-number. In methanol, acetaldehyde is formed in ppm range but is factor of 2 higher in ethanol and butanol. The complete experimental datasets of methanol, ethanol, and n-butanol are provided as supplemental material.

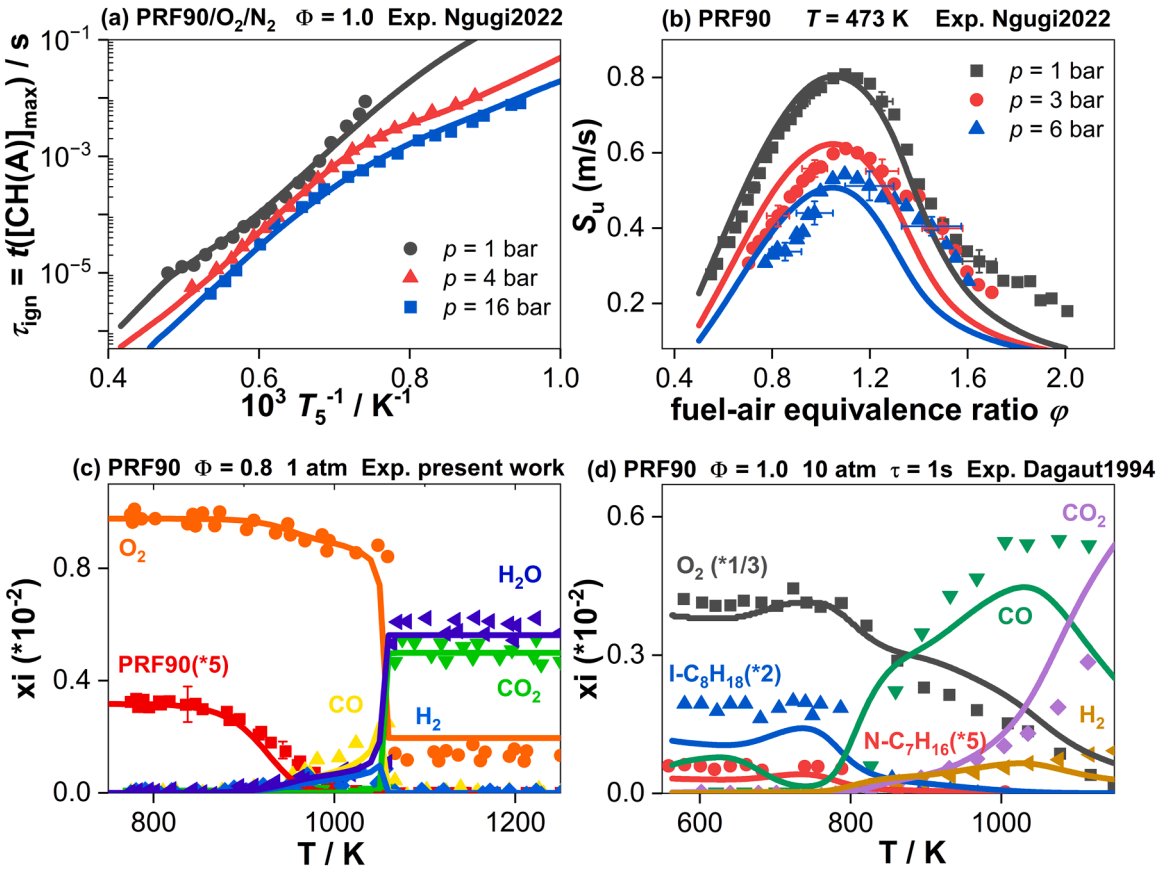

Fig. 13. Validation of PRF90 against (a) ignition delay times [33], (b) laminar flame speeds [33] and major species in (c) DLR flow reactor, and (d) JSR [83]. All data are formulated surrogate PRF90. Scaling factor indicated when applied.

3.3. Fuel surrogates – gasoline surrogate, diesel surrogate

OMEs are often regarded to be used in conventional fuel blends in studies and real applications. To understand the combustion properties of OMEs blended with gasoline or diesel fuels, a model for their fuel surrogate is also necessary. The model validation of both these fuel surrogates is presented in Figs. 13 and 14. A new speciation dataset for simple gasoline surrogate PRF90 (11.1 mol% n-heptane + 88.9 mol% iso-octane) oxidation is obtained in a high-temperature flow reactor at four stoichiometries (Φ = 0.8, 1.2, 1.43, and 2.0) and is available as supplemental material. Fig. 13 shows that the fuel and oxidizer consumption and major products are well captured by the model. Additionally, PRF90 was measured in a JSR at 10 atm pressure and at low to high temperatures by Dagaut et al. [83]. The model is capable to predict the decrease in reactivity at lower temperatures observed in the JSR. Furthermore, laminar flame speeds obtained at 473 K up to 6 bar [33] and IDTs at high temperatures (Φ = 1.0, 1–16 bar) [33] add to the model validation, both of them are well predicted by the model. Other gasoline surrogates are presented in supplemental material in **Fig. S17**.

Combustion characteristics of diesel is modeled using diesel surrogate (50 mol% n-dodecane + 30 mol% farnesane + 20 mol% 1-methylnaphthalene) and is presented in Fig. 14. The ignition delay times of DF-2 measured in high-temperature range [84] are well predicted by the above specified surrogate. The DF-2 is a diesel fuel from the U. S. Army Propulsion Laboratory [84]. The laminar flame speeds of the above defined diesel surrogate are obtained at 473 K preheat temperature and up to 6 bar pressure [65]. The model reproduces the laminar flame speeds within the uncertainty limits of the measurements. Additionally, various C_1-C_6 hydrocarbon intermediates were measured in a JSR by Mati et al. [85] at 10 atm using synthetic diesel. The synthetic diesel is comprised of 23.4 mol% n-hexadecane, 18.9% iso-octane, 26.9% n-propylcyclohexane, 22.9% n-propylbenzene, and 8% 1-methylnaphthalene which is also used in model. The model also well predicts the aromatic benzene and toluene formed from synthetic diesel as well as some of the C_4-C_6 intermediate species as shown in Fig. 14.

4. Results and discussion – relative reactivity of OMEs

Due to structural difference of OMEs compared to respective hydrocarbons, a change in product distribution of various pollutants is expected. Examples are a decrease in PAH and soot emissions or increase in formation of oxygenated compounds such as aldehydes.

This section compares relative reactivity of OMEs by first comparing their global reactivity, followed by the effect of chain-length using different intermediates and products formed in the oxidation of OMEs. Furthermore, NO_x chemistry an important aspect of transportation fuel consumption where the synergetic effect of OME and NO chemistry on NO_x formation is presented. In addition, the effect of mixing OME to hydrocarbons is also discussed, an important aspect for fuel blending. For such systematic insights, availability of experimental evidences of various OMEs at same combustion condition as well as capable model is necessary.

4.1. Comparison of global reactivity

Although various combustion characteristics of OMEs are investigated both experimentally as well as numerically, a comparison of relative reactivity of series of OMEs is presented in brief and requires attention. Fortunately, by now, adequate measurements are available, allowing direct comparison and systematic discussion of various aspects

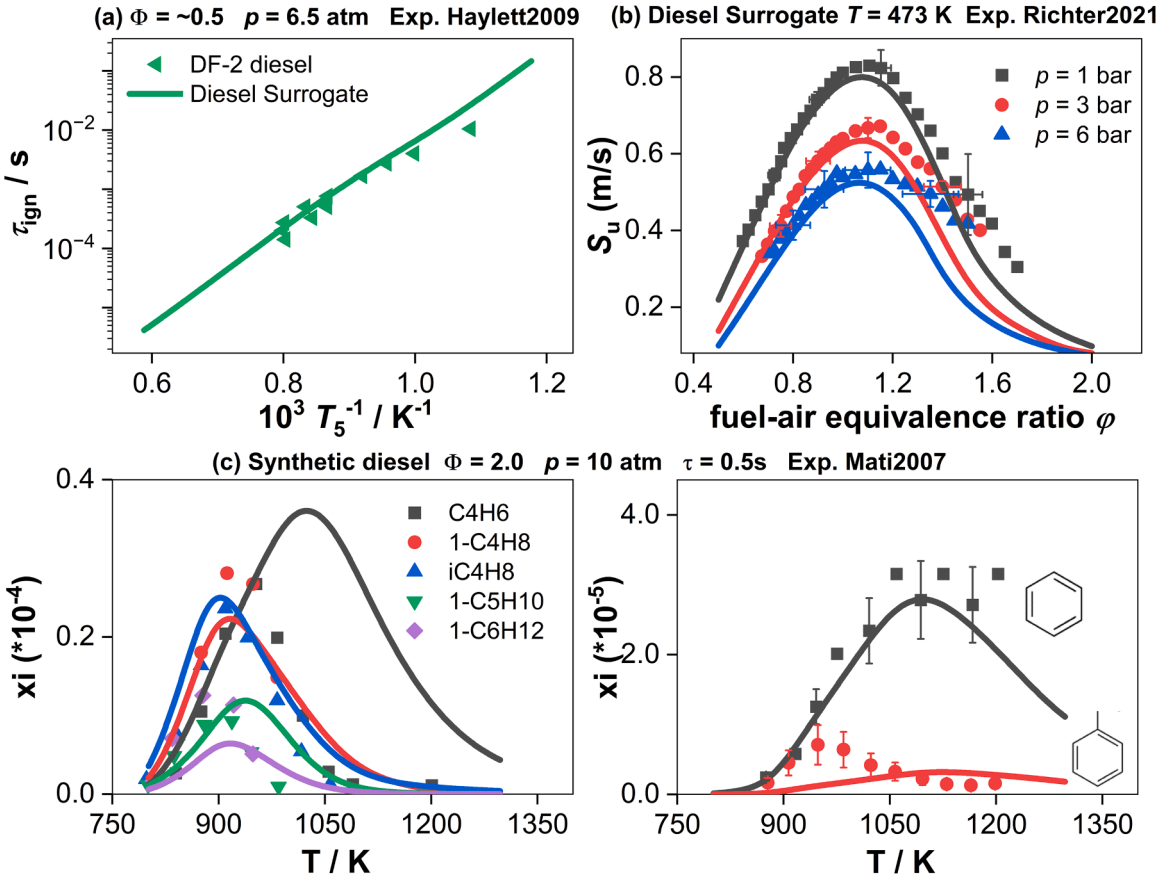

Fig. 14. Comparison of measured (symbols) and modeled (curves) diesel and diesel surrogate: (a) ignition delay times [84], (b) laminar flame speeds [65], and (c) species in JSR [85].

of OMEs.

In Fig. 15, the global reactivity of OMEs, at a given condition, is compared in different combustion setups. This figure covers reactivity of OME0-5 at wide variety of combustion conditions obtained in shock tubes, laminar flames, as well as jet-stirred and flow reactors. The general consensus among these data is (1) reactivity of OMEs at all temperatures increases with increase in OME chain-length but this increase is not linear, (2) at low temperature and in the NTC, decrease in reactivity is observed where OME1 presents weak feature compared to OME≥2, (3) reactivity of OME0 and OME1 differs from larger OMEs, and (4) reactivity of OME≥2 is nearly indistinguishable. Similar interpretations are also done earlier in individual experiments with selected OMEs mostly OME0-3 [44,40,31,32,35,34] but a comprehensive picture as such in Fig. 15 has not been presented before.

The analysis with DLR Concise shows that the reactivity of the OMEs at all temperatures is mainly governed by (1) primary radicals and (2) methoxymethylene formates ($CO(CO)_xCHO$, where x ≥0), as shown in Fig. 16. Regardless of chain-length, at high temperatures the thermal decomposition predominantly leads to primary OME_{x-1} radicals which further decomposes to smaller *p*-OME_{x-x} radicals. At other temperatures, again primary radical first through H-atom abstraction to *p*-OME_x and then dissociates to smaller primary radicals *p*-OME_{x-1} through ß-scission. These routes are consistent among OMEs. Second important species in OME system are the formic acid esters ($CO(CO)_xCHO$) such as methyl formate (x = 0), methoxy-methyl formate (x = 1) and further larger esters named in general as methoxymethylene formates. The methoxymethylene formates are formed during ß-scission of secondary fuel radicals or at NTC and low temperatures from KHP decomposition. A sensitivity analysis to support this is available in **Fig. S2.1-S2.3** as supplemental material.

At intermediate and low temperatures, the formation of $CO(CO)_xCHO$ from *s*-OME_{x-1}, due to low energy barrier, is so dominant that it successfully competes with low-temperature peroxy chemistry of secondary fuel radicals. Thereby making the low-temperature peroxy chemistry of secondary radicals insignificant (see e.g. **S2.8**). This information is useful for smaller semi-detailed models which can neglect these routes without affecting the global reactivity. For example, in DLR Concise we achieve 60% reduction in number of species (90 species) in low temperature route without significant effect on reactivity (see **Figs. S64, S65, S67** in supplemental material). The presence of $CO(CO)_xCHO$ has subsequently global inhibiting effect at NTC and low temperatures. At low temperatures, the reactivity increases through the decomposition of KHP which is a chain branching reaction releasing hydroxyl radical and methoxymethylene formates. Thus, the global reactivity of OMEs seems to be governed by balance between their primary radicals and $CO(CO)_xCHO$ chemistry whose concentration increases with increase in chain-length (OME≥1). Since no methoxymethylene formates are formed in OME0, their chemistry is dominated by primary radicals and differs most from other OMEs.

The difference in reactivity of OMEs at low temperatures can also be interpreted from its difference in the H-transfer possibilities during isomerization reactions of RO_2 to QOOH which leads to the chain branching forming two hydroxyl radicals. Number of such possible ring transitions is listed in Table 3. An important aspect is the position of carbon atom between which the H-atom is migrating i.e. at primary or secondary positions (for list of possible transitions in OME0-OME5 see **Fig. S107** in Supplemental material). In case of linear OMEs, tertiary carbons are not present. In contrast to alkanes, the BDEs of *p*(C-H) is lowest which encourages the O_2 addition at this position which also determines the fate of degenerating branch and the global reactivity. As shown in Vermeire et al. [24], the bond enthalpy at 298 K of O_2 addition to primary radical (148 kJ mol^{-1}) is lower than to secondary radical (164 kJ mol^{-1}). As discussed earlier, the primary radical route dominates the (low *T*) chemistry. Considering number of ring transitions that can occur from secondary carbon atom to primary carbon position connected to -OOH site (*s-p*) shows (see **Fig. S107** in Supplemental material), no such transition is feasible in DME, one such transition is possible in OME1 whereas for OME≥2 two *s-p* ring transitions are seen (Table 3), which is consequently reflected in the global reactivity. However, recent work by De Ras et al., [69] shows completely different behavior of OME2. They showed that even though the primary C-O bond is the weakest, the enthalpy of formation of primary and secondary fuel radical is nearly similar. In addition, they calculated the energy barrier of O_2 addition to OME2*-5 radical to be lowest which accounts for *s-s* transition in Table 3. Unfortunately, there is no other information available on larger OMEs for comparison. Therefore, in absence of appropriate potential energy information of higher OMEs it is not possible to examine the general low-temperature reactivity based on H-transfer activity of OME molecule. Additionally, the *s-s* ring transitions which are present in increasing number with increase in OME chain has no effect on global reactivity.

4.2. *Influence of molecular structure – Chain-length, (-CH_2O-) unit*

Understanding of the influence of molecular structure of OMEs due to their varying chain-length or degree of polymerization as well as effect of presence of oxygenated functional group (-CH_2O-) can be important for fuel characterization and emission formation. There are three aspects that require attention here: (1) absence of C-C bond, (2) presence of C-O bond, and (3) number of C-O bonds (= chain-length).

Although these aspects are interrelated, they have varying impact on different pollutant formation. The absence of C-C bond is expected to play an important role in soot particle reduction among OMEs which has been observed in [86]. In this work, premixed flames of neat ethylene and ethylene blended with OME2-4 are investigated at constant cold gas velocity, with 20% of total carbon substituted by OMEs. The temperature profiles of neat and blended flames are identical allowing to focus on OMEs specific influence on soot variation rather than thermal effects. The reduction of C-C bonds leads to reduction in number and size of soot particles, but the number of C-O bonds (effect of chain-length) was found to be negligible on soot reduction [86]. On the other hand, the presence and number of C-O bonds may have adverse consequence of possible increase of non-regulated oxygen containing pollutants such as aldehyde components. Also, there is aspect of NO_x formation, indirectly effected by changed combustion temperatures.

The most consistent intermediates present in all the OMEs are formations of formaldehyde and methyl radicals, which also control the reactivity. Both are produced predominantly from fuel radicals as shown in Fig. 17. The formaldehyde is produced from all primary fuel radicals (*p*-OME_{x-1}) involved in the process. Thus, the longer the OME chain-length, the higher is the amount of CH_2O released on a molar basis. In the NTC and low temperatures, the influence of peroxy chemistry can complicate the matter where the relation may not be straight forward.

In comparison, the CH_3 radical is formed from decomposition of methoxy methyl radical (CH_3OCH_2) and from secondary fuel radicals at any third carbon position formed in the series. In OMEs compared to hydrocarbons, primary radical reactivity is more dominant compared to secondary radical (Fig. 2). Therefore, the dependence of chain-length is more visible on CH_2O formation compared to the formation of CH_3 radicals.

The effect of OME chain-length on the formation of above discussed two species can be observed from our flames [34] and reactor [35] experiments measured with constant cold gas velocity and constant carbon flow, respectively, for various OMEs (Fig. 18). Here, at flame conditions, the increase in chain-length leads to increased CH_2O mole fractions whereas the mole fraction of CH_3 decreases from OME1 to larger OMEs. A similar comparison in OME1-3 in stoichiometric flames in only modeled data of Sun et al. [27] showed a decrease in CH_3 and an increase in CH_2O mole fractions. In absence of contributions from secondary fuel radical not available in DME, the amount of CH_3 formed in DME is less than OME1 contrary to expected in the series. This is consistent with data from flow reactor [35] and in shock tube [64].

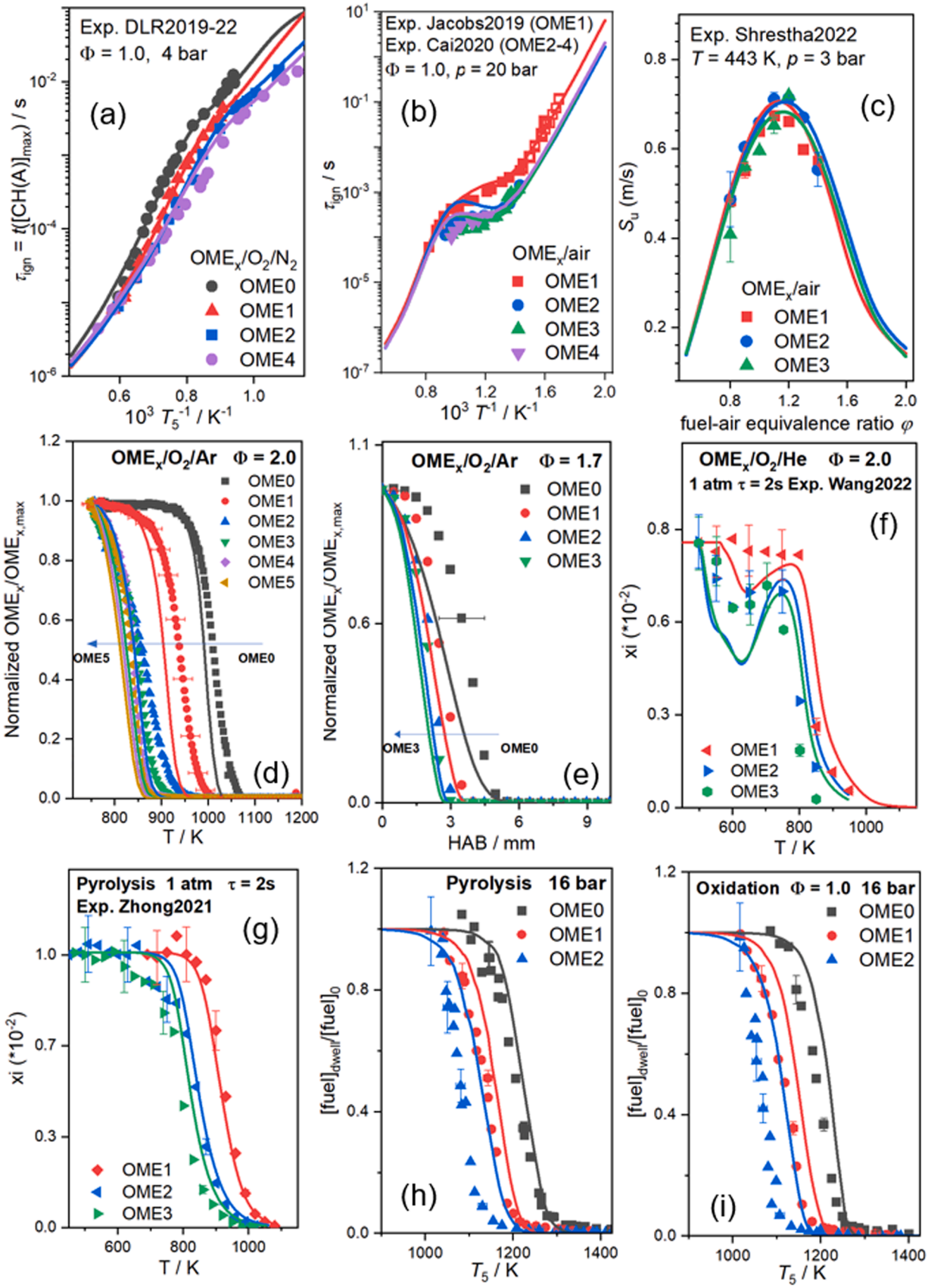

Fig. 15. Comparison of global reactivity of OMEs in different combustion setups: (a,b) ignition delay times [63,31,25], (c) laminar flame speeds [32], (d) oxidation in flow reactor [35], (e) burner-stabilized flames [34], (f) oxidation in JSR [44], (g) pyrolysis in JSR [40], (h) pyrolysis in shock tube [64], and (i) oxidation in shock tube [64].

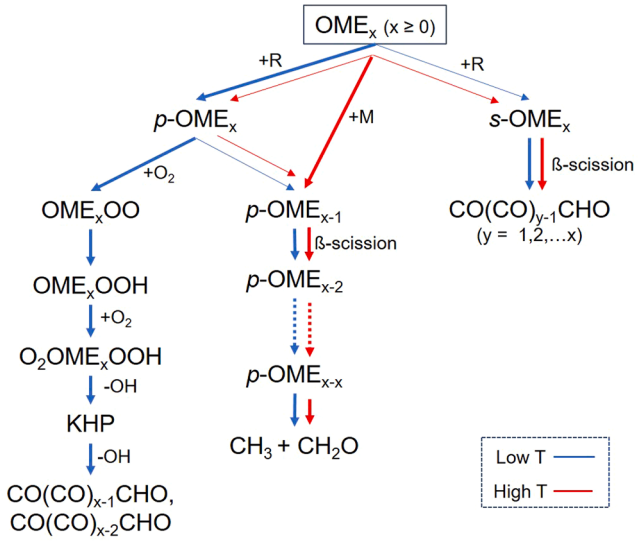

Fig. 16. Dominance of primary fuel radicals and methyl formates on global reactivity of OMEs.

4.3. *Effect of blending with hydrocarbons*

DME as ignition enhancer for methanol fueled engines [87] or its suitability for improved combustion performance in diesel engines [88] has shown potential of DME as blending component. A future use of DME in gas turbines for power generation, including necessary nozzle modifications, was demonstrated in [89,90]. In general, several studies are dedicated to the understanding of combustion characteristics and potential emission behavior of OMEs-hydrocarbon blends [16,17,21,33,47,65,81,91–101]. These studies identify significant decrease in the IDTs of hydrocarbons in presence of OMEs. However, the relative reactivity among hydrocarbons differs depending on their molecular structure and C-H bond strength.

Studies on the effect of DME addition to methane mixtures have shown that DME has significant impact on the ignition behavior of blends with CH_4 [101,93,92,95,17,16]. In fact, enhanced ignition effect of DME addition to CH_4 was found to exceed that of equivalent H_2 addition [93] and the effect of blending is non-linear. A small amount of DME added to methane showed considerable reduction of IDTs as presented in Fig. 19 where the DME chemistry controls the mixture reactivity. However, as the blending ratio increases the reduction in IDTs is not as strong as at lower DME concentrations. In Fig. 19, the effect of 40% DME addition to methane on reactivity is not far from 20% DME blend. The increased reactivity of DME is caused by the quick conversion

Table 3
Number of ring transitions during RO_2 to QOOH isomerization in OME0-OME5.

Fuel \ Ring Transition	*p-p*	*p-s*	*s-p*	*s-s*
OME0	1(6)	-	-	-
OME1	1(8)	1(6)	**1(6)**	-
OME2	-	1(6), 1(8)	**1(6), 1(8)**	1(6)
OME3	-	1(6), 1(8)	**1(6), 1(8)**	2(6), 1(8)
OME4	-	1(6), 1(8)	**1(6), 1(8)**	3(6), 2(8)
OME5	-	1(6), 1(8)	**1(6), 1(8)**	4(6), 3(8)

Nomenclature: p: primary, s: secondary

p-s: p (carbon position) to *s* (carbon position of O-O)
1(6): one such 6-ring transition

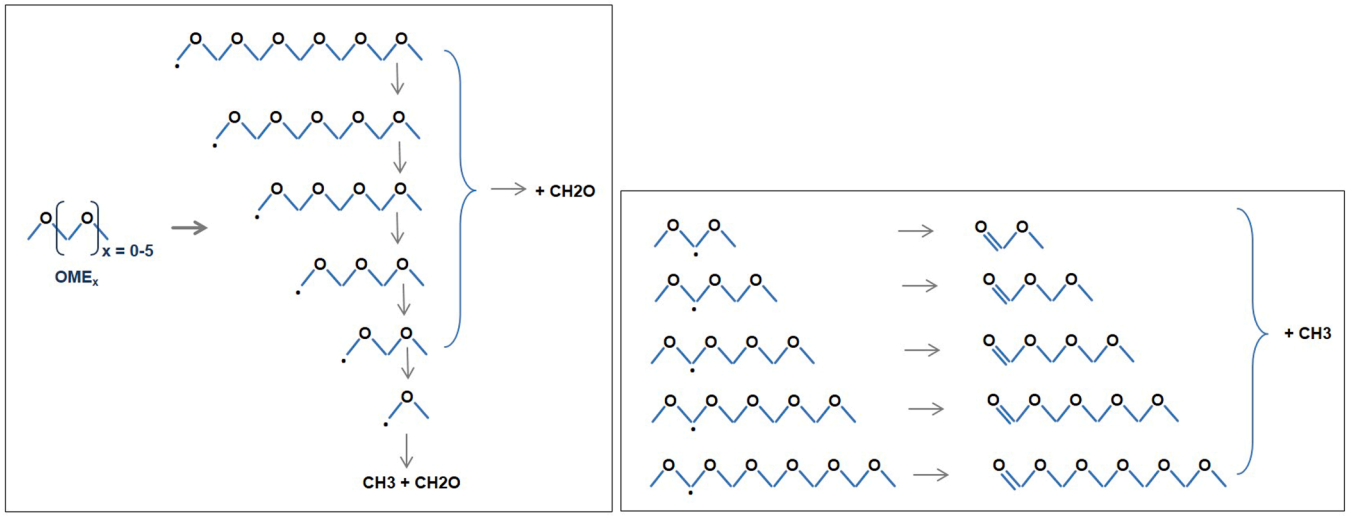

Fig. 17. Reaction sequence involved in formation of CH_2O and CH_3 radicals from OME_x fuel.

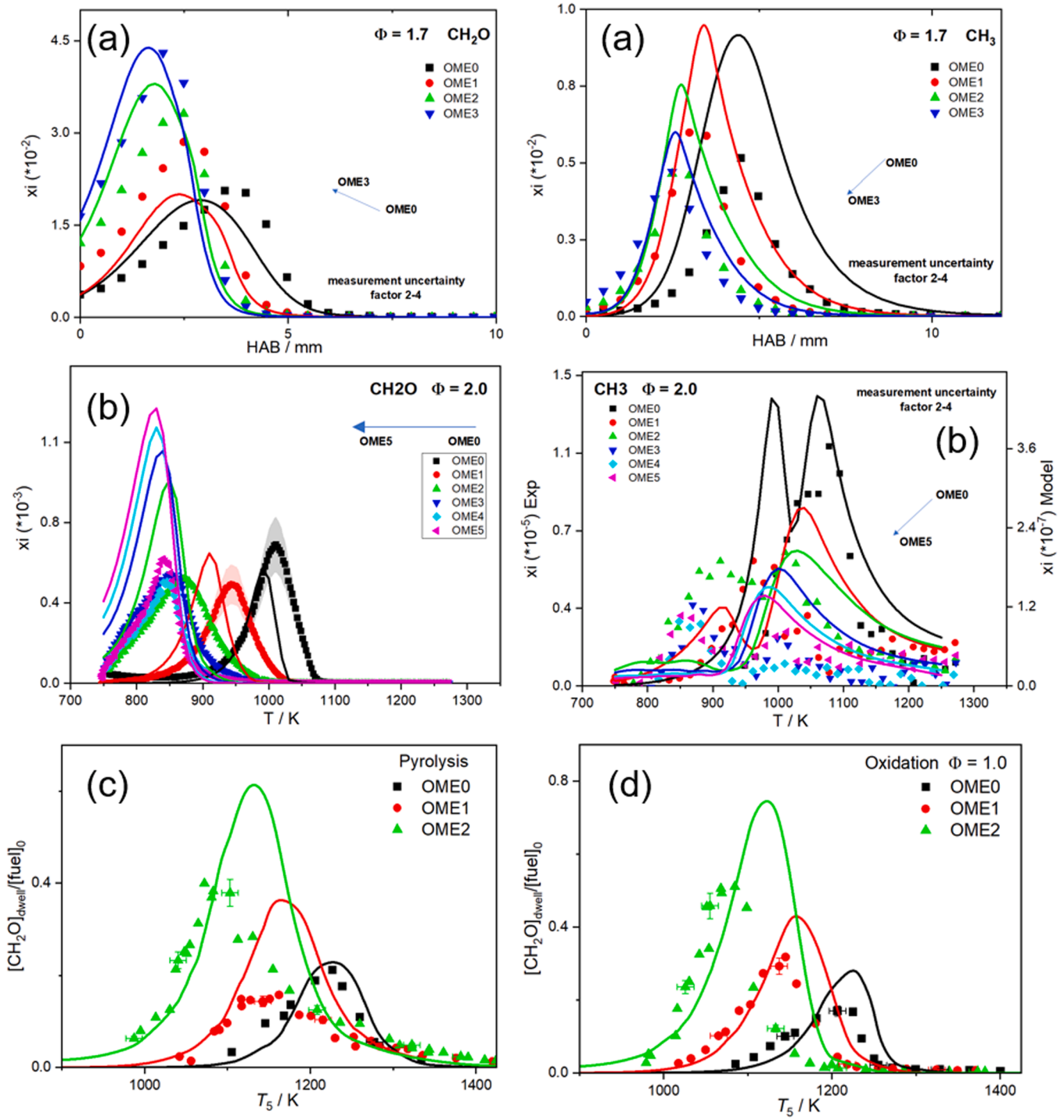

Fig. 18. Effect of molecular structure on CH_2O and CH_3 formation at various combustion conditions and setups: (a) burner-stabilized flames [34], (b) flow reactor [35], (c) pyrolysis, and (d) oxidation in single pulse shock tube [64].

of DME by ß-scission to formaldehyde (and CH_3 radicals) that generates more radical pool compared to methane (which has relative stable C-H bonds) converting to CH_3 radicals. A mixture of DME and toluene (as alternative component of primary reference fuel) shows linear change in IDTs with DME addition.

In case of OME1 and n-heptane mixtures, the ignition delay time enhancement is nearly linear to the amount of OME1 added. Fig. 19 shows that the IDTs reduces to 50% when about of 70% OME1 blended with PRF90 which is primarily iso-octane (90%). Both n-heptane and iso-octane (in PRF90) show similar reduction in IDTs in presence of OME1, with the overall enhancement effect slower than seen in DME-CH_4 mixtures.

In DME-CH_4 flames, as pointed out in [93], the influence of OMEs in hydrocarbon is less prominent in transport driven regime. Compared to non-linear increase in IDTs, the increase in flame speed is noted to be linear with DME addition. As shown in Fig. 20, the laminar flame speeds of DME-CH_4 mixtures and OME1 and OME4 added to PRF90 and diesel surrogate respectively show no drastic effect on the flame speeds.

The addition of OMEs to hydrocarbon significantly enhances the reactivity of the blend specially in the NTC as seen in Fig. 19. Their

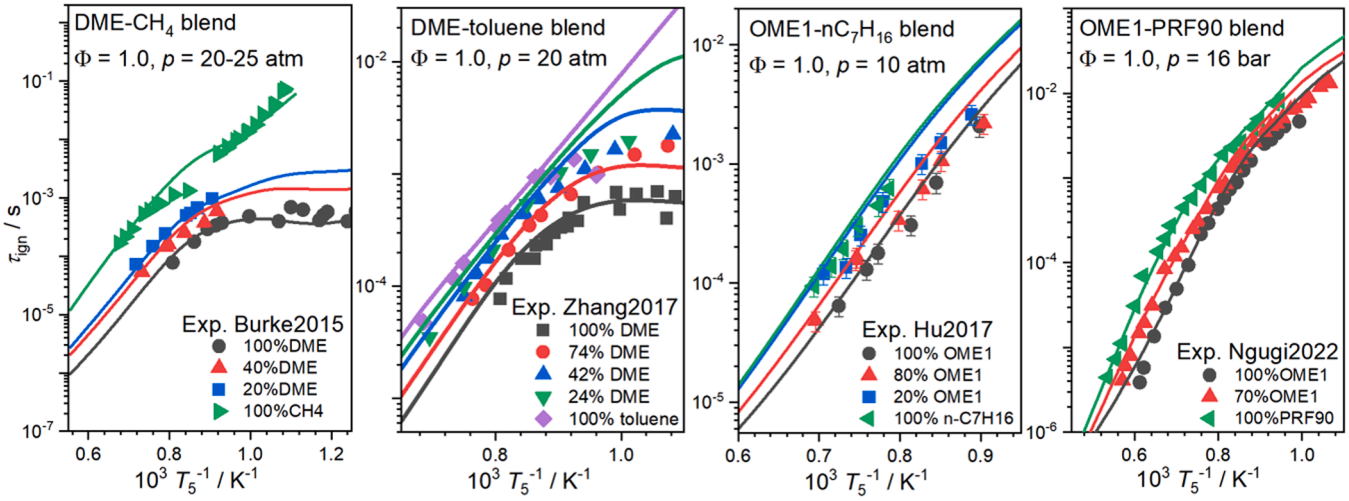

Fig. 19. Impact of DME and OME1 addition on IDTs of hydrocarbons: DME-CH_4 [16], DME- toluene [97], OME1-n-heptane [21], and OME1-PRF90 [33].

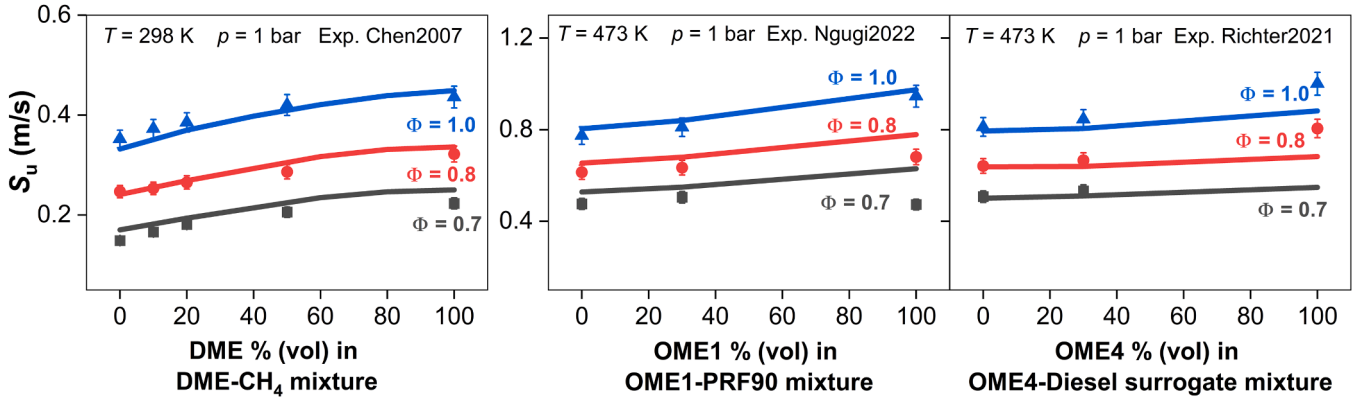

Fig. 20. Impact of OME addition on laminar flame speeds of hydrocarbons: DME-CH_4 [93], OME1-PRF90 [33], and OME4-Diesel surrogate [65].

reactivity can be interpreted by the OH radical pool formed as shown in **Fig. S2.5**. The OMEs generates early OH radical pool compared to hydrocarbons for e.g. n-heptane or toluene. This is due to fast buildup of CH_3 radicals from methoxy radicals and secondary fuel radicals, as shown in **Fig. S2.5** in supplemental, whereas in n-heptane and toluene this occurs mainly when smaller radicals are subsequently formed from the fuel. In case of toluene, CH_3 radicals are also scavenged by stable species. Thereby the reactivity of OMEs is determined by primary radicals and $CO(CO)_xCHO$ formed and their chemistry will dominate in blends with high amount of OMEs.

4.4. NO-OMEx sensitization

Exhaust gas recirculation (EGR) can serve as an effective way to reduce pollutants in combustion engines (spark-ignition (SI), compression-ignition (CI) engine). This method unintentionally also introduces temperature active NO_x species into the combustion chamber. Chemical interaction of hydrocarbon fuels in presence of NO species and its influence on chemical reactivity of hydrocarbons specially at low and intermediate temperatures is well studied [92,102,103]. In hydrocarbons at low temperatures, the presence of NO provides source of chain carriers through the reaction $CH_3O_2 + NO = CH_3O + NO_2$ where methyl-peroxy radical is no longer chain terminating [104]. This reaction dominates the fuel oxidation. Studies have shown similar influence on the reactivity of DME in presence of NO.

Few experimental investigations are carried out in flow reactor on DME-NO [92,15,105,106,39,18,32] and OME1-NO [39] mixtures. Given the significance of OMEs in transportation fuel, surprisingly few models are dedicated to DME-NO_x modeling [15,105,106,39,18,32] and no experimental or numerical investigations are reported for higher OMEs sensitization through NO. Studies on DME oxidation have shown that the addition of NO [15,105,39,18,32], NO_2 [15,106] and NH_3 [107,108] significantly effects the oxidation rate of DME. Experimental investigations in flow reactor have proofed inhibiting effect of NO in DME at lower temperatures and promoting effects at high temperatures [15,105,39,18]. The only measurement on OME1 also shows similar effect on the reactivity of OME1 in presence of NO [39].

As listed in Table 4, in DLR Concise, the interaction of the DME with NO_x is mainly described by two types of reactions (1) DME + $NO/NO_2/NH_2$/CN = DME*-1 + RH, and at low temperatures (2) DME*-1OO + NO/HONO = A + NO_2. Fig. 21 shows DME conversion in presence of NO in a flow reactor for temperatures of 430–950 K at atmospheric pressure measured by [39]. It shows that the overall reactivity of DME increases

Table 4
OME_x-NO sensitization reactions included in the mechanism (x = 0–5).

OME_x-NO	$OME_x + NH_2 = OME_x$*-1 + NH_3
	$OME_x + CN = OME_x$*-1 + HCN
	$OME_x + NO = OME_x$*-1 + HNO
	$OME_x + NO_2 = OME_x$*-1 + HONO
	OME_x*-1OO + NO = $CO(CO)_xCO$* + NO_2
	OME_x*-1OO + HONO = $CO(CO)_xCO$* + OH + NO_2

Analogous reactions implemented for OME_x (x > 1), in absence of any experimental data currently not validated.

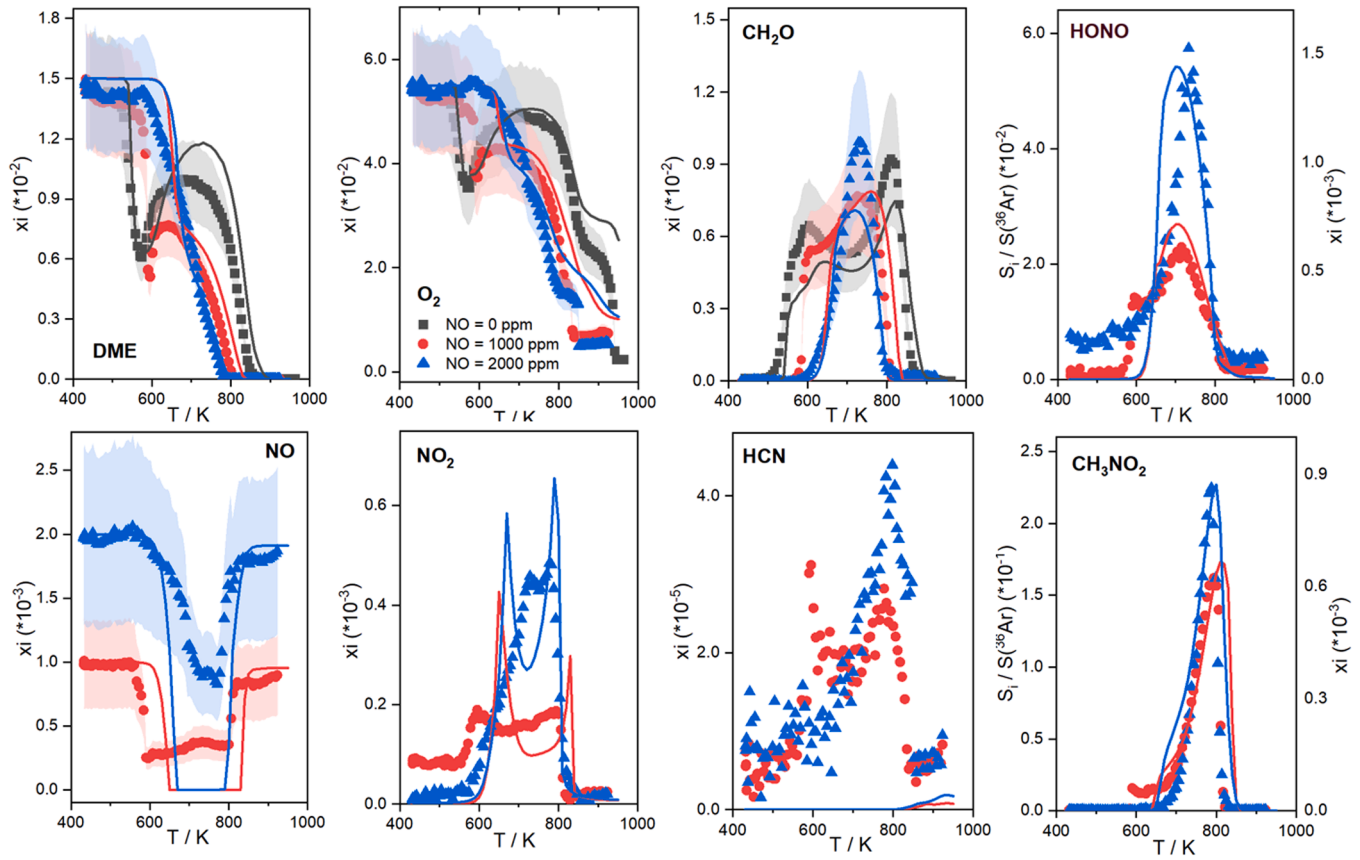

Fig. 21. Influence of NO on DME combustion in low to intermediate temperatures in flow reactor [39] for DME, DME+1000ppm NO, DME+2000ppm NO mixtures at $\Phi = 0.8$ and 0.97 bar pressure.

as the NO concentration in the fuel-oxygen mixture is increased. However, in the low-temperature and NTC region the reactivity of DME is inhibited in the presence of NO [39,18]. In addition, the model also reproduces the oxygenates formaldehyde and methyl formate (**Fig. S33**, supplemental material). The consumption of NO and subsequent formation of NO_2 in the model is mostly within the uncertainty limit. The model however does not reproduce elevated NO concentrations at intermediate temperatures, which could possibly be result of multiple species fragmentations as discussed in [18]. The profile shape and peak position of CH_3NO_2 and HONO are accurately reproduced by the model compared to their respective signals in Fig. 21.

The formation route of HCN measured from NO sensitization is unclear. Alzueta et al. [15] reported minor concentration of HCN above 1100 K and none below. This was observed in our simulations of Zhang et al. [39] data where above 850 K, the HCN formation from prompt NO route is seen to be formed by the mechanism but not at lower temperature. Considering DME-NO sensitization reaction DME*-1 + NO = HCN + CH_2O + H_2O (with reaction rate from analogy of CH_2HCO + NO = HCN + HOCHO) sees the formation of HCN at lower temperatures. As more experimental investigations are necessary in this direction, no reactions are included in our model in the given state.

To our knowledge, among OMEs only DME-NO interaction is currently implemented in literature mechanisms [15,105,106,39,18,32]. To this end, we applied DME-NO analogy to the OME1-NO reaction system. The reactions analogous to DME are (1) OME1 + NO/NO_2/NH_2/CN = OME1*-1 + RH and (2) OME1*-1OO + NO/HONO = A + NO_2. The Fig. 22 shows influence of NO on the reactivity of OME1 measured in atmospheric flow reactor [39], at conditions similar to DME data presented in Fig. 21. The presence of NO-OME1 sensitization reactions in model shows considerable improvement compared to when no interaction is considered. The predictions of nitrogen containing species are similar to DME and are well predicted by the model.

Additionally, ignition delay times of DME-NO_2 interactions measured in [106] are shown in Fig. 23. The addition of NO_2 increases the reactivity of the blend leading to faster IDTs. The model comparison reproduces the effect of NO_2 blending excellently, which is more prominent at lower temperatures compared to high temperatures.

To conclude our exhaustive presentation and discussion of the DLR Concise, perspectives for future analysis are mentioned here briefly. Foremost, the attractiveness of oxygenates in general as a fuel is due to the strong C-O bond, which never becomes involved in soot formation pathways. During the ignition process, the C-O bond remains unbroken and instead, in sequence of steps, it is converted to CO via CH_2O. As seen in Fig. 24, this can result in increased CO, CO_2, HCO, and CH_2O maximum mole fractions with increase in OME chain-length. As expected, the amount of soot precursors and PAH formed in OMEs decreases with increase in OME chain-length.

Various engine studies have shown benefits of using OMEs through changes in operating points or impact of exhaust gas recirculation on NO_x and soot emissions. A change in a single aspect can lead to different or sometimes contradicting results such as increase in EGR rates leads to reduction in NO_x emissions due to reduced temperatures, but also increase in sooting tendency as the EGR causes decrease in excess air [61]. Blending of OMEs may help avoid local fuel-rich regions in such cases.

In general, identifying and customizing combination of operating and combustion conditions can supply suitable solution towards sustainable and low- to zero-emission fuel in combustion applications. The multi-component reaction model as such DLR Concise presented in this study can serve as starting point for such model-based design and analysis to emulate different operating points and can suggest operating conditions for optimal operation along with NO_x and particulate reduction.

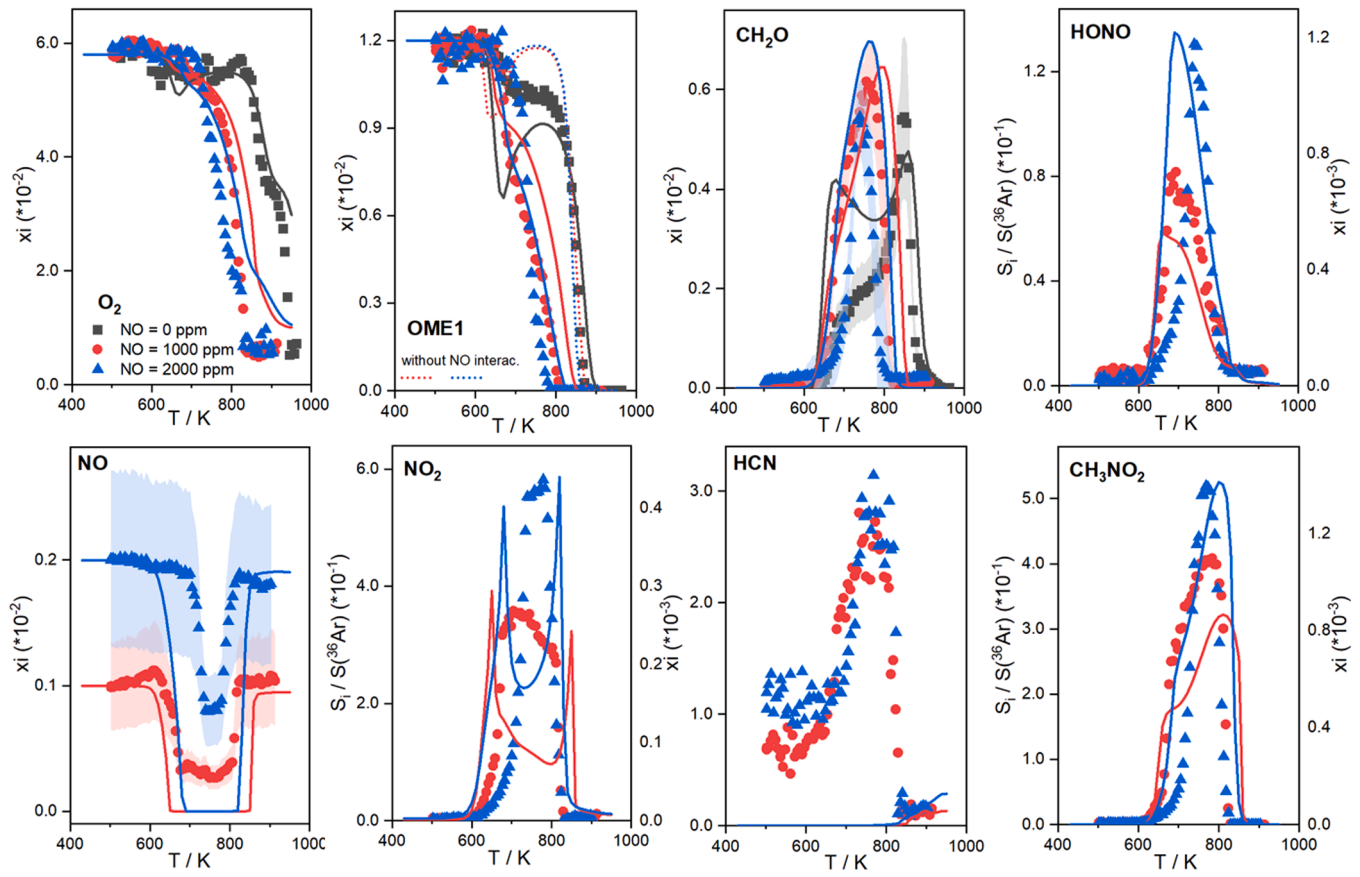

Fig. 22. Influence of NO on OME1 combustion in low to intermediate temperatures in flow reactor [39] for OME1, OME1+1000ppm NO, OME1 + 2000ppm NO mixtures at Φ = 0.8 and 0.97 bar pressure.

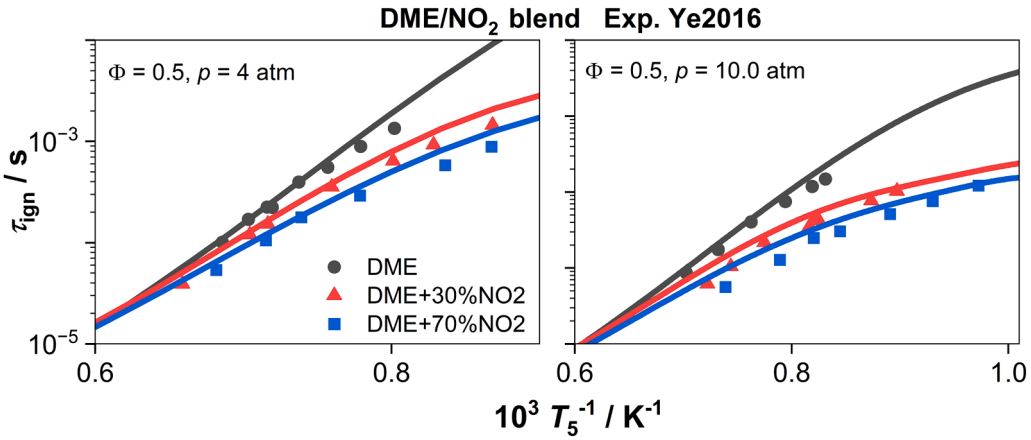

Fig. 23. Influence of NO_2 on DME ignition delay times measured in shock tube. Measurements performed at Φ = 0.5, with DME and DME blends with 30, 70 (mol)% NO_2 [106].

5. Concluding remarks

In this work, we extend our previously published reaction mechanism (DLR Concise) to include components to describe a range of transportation fuels. The DLR Concise is intended as a single flexible reaction model for alternative fuel surrogates; its target application is both aviation- as well as transportation-fuel surrogates. A major part of the work discusses the reaction kinetics of oxymethylene ethers (OME_x, x = 0–5) from high to low temperatures relevant for engine conditions in transportation and is extensively validated for wide range of combustion conditions by using in-house as well as large amount of literature data. On a side note for a broader application range, the reaction mechanism also includes kinetics of gasoline- and diesel-surrogates, and alcohols (C1-C4) relevant for road transport fuels.

Due to availability of multiple components of various molecular structures, emission components of NO_x as well as PAH, and reasonably small number of species, all in a single mechanism - the DLR Concise provides convenient opportunity for model-based fuel assessments and optimization studies, both in simple and complex engine/combustor geometries.

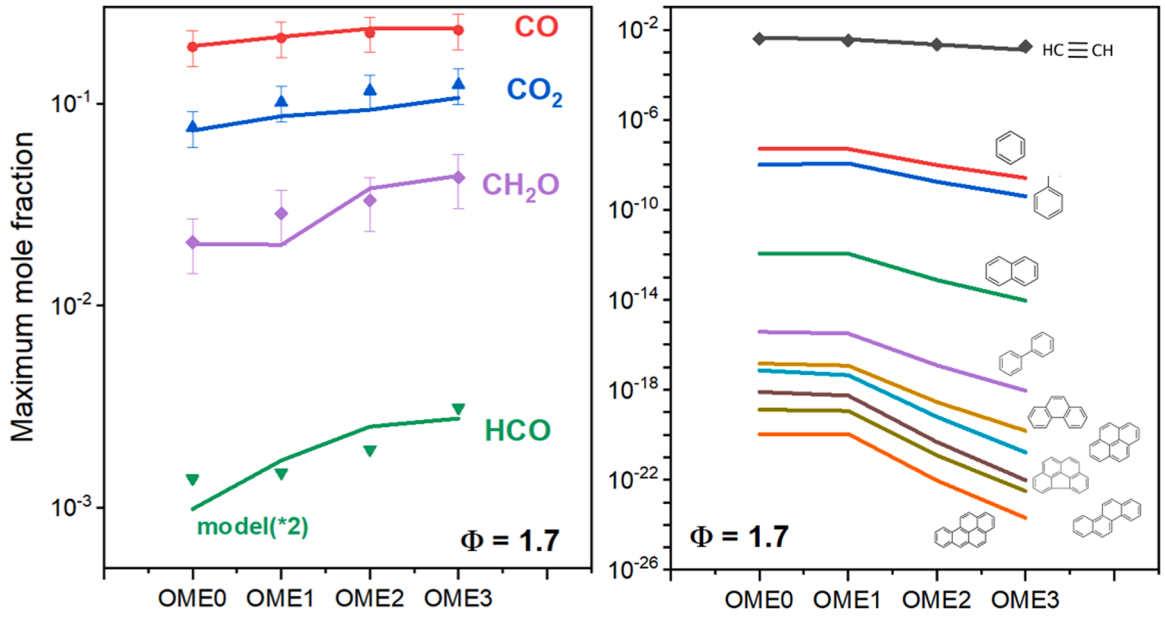

Fig. 24. Change in mole fractions of oxygenated and soot precursor species in OME0-3 burner-stabilized flames [34]. Symbols: experiments, lines: simulations. No measurements available for aromatics, only modeled data shown.

Novelty and significance statement

The main focus of this work is the detailed description of reaction kinetics of oxygenates (alcohols, OME0–5) through the extension of reaction mechanism "DLR Concise" that includes variety of H/C/O/N components. The novelty of this research is, starting with the detailed reaction kinetics we also cover range of topics related to OMEs such as influence of molecular structure, effect of blending with hydrocarbons, as well as NO_x-OME sensitization to discuss the reactivity of oxygenates. The reaction model presented in this work is extensively validated against wide-ranging experiments both in-house and from literature.

The DLR Concise is a flexible reaction model which supplies as many possible components of diverse molecular structure with semi-detailed chemistry to model a spectrum of aviation and transportation fuels. As a result, this comprehensive work provides a single reaction model for fuel assessment and optimization of neat and blends of various hydrocarbon and oxygenated compounds and predict PAH and NO_x emissions.

Supplemental material

This document contains extensive supplemental material. The DLR Concise is available as supplemental material as well as in public domain at: https://www.dlr.de/vt/mechanisms

CRediT authorship contribution statement

Trupti Kathrotia: Writing – original draft, Validation, Methodology, Investigation, Formal analysis, Conceptualization. **Thomas Bierkandt:** Writing – review & editing, Investigation. **Nina Gaiser:** Investigation. **Sandra Richter:** Investigation. **Fabian Lindner:** Investigation. **Sascha Jacobs:** Writing – review & editing. **Clemens Naumann:** Supervision, Investigation. **Torsten Methling:** Writing – review & editing, Software, Funding acquisition. **Patrick Oßwald:** Writing – original draft, Supervision, Investigation. **Markus Köhler:** Writing – original draft, Supervision, Funding acquisition.

Declaration of competing interest

The authors declare that they have no known competing financial interests or personal relationships that could have appeared to influence the work reported in this paper.

Acknowledgment

The authors gratefully acknowledge the DLR projects NeoFuels and Future Fuels for providing the framework of this comprehensive work. Fabian Lindner gratefully acknowledges Friedrich and Elisabeth Boysen Foundation (project ID: BOY-140) for research funding. Authors thanks Dr. Steffen Schmitt for review and constructive comments.

Supplementary materials

Supplementary material associated with this article can be found, in the online version, at doi:10.1016/j.combustflame.2024.113841.

References

[1] K. Kohse-Höinghaus, Combustion in the future: the importance of chemistry, Proc. Combust. Inst. 38 (2021) s6.
[2] L. Cai, F. vom Lehn, H. Pitsch, Higher alcohol and ether biofuels for compression-ignition engine application: a review with emphasis on combustion kinetics, Energy Fuels 35 (2021) 1890–1917.
[3] K. Kohse-Höinghaus, Combustion, chemistry, and carbon neutrality, Chem. Rev. 123 (2023) 5139–5219.
[4] D. Bongartz, J. Burre, A. Mitsos, Production of oxymethylene dimethyl ethers from hydrogen and carbon dioxide-Part I: modeling and analysis for OME1, Ind. Eng. Chem. Res. 58 (2019) 4881–4889.
[5] J. Burre, D. Bongartz, A. Mitsos, Production of oxymethylene dimethyl ethers from hydrogen and carbon dioxide-Part II: Modeling and analysis for OME3–5, Ind. Eng. Chem. Res. 58 (2019) 5567–5578.
[6] A. Oyedun, A. Kumar, D. Oestreich, U. Arnold, J. Sauer, The development of the production cost of oxymethylene ethers as diesel additives from biomass, Biofuels Bioprod. Bioref. 12 (2018) 694–710.
[7] S. Schemme, R. Can Samsun, R. Peters, D. Stolten, Power-to-fuel as a key to sustainable transport systems – an analysis of diesel fuels produced from CO2 and renewable electricity, Fuel 205 (2017) 198–221.
[8] Y. Fenard, G. Vanhove, A mini-review on the advances in the kinetic understanding of the combustion of linear and cyclic oxymethylene ethers, Energy Fuels 35 (2021) 14325–14342.
[9] A. Fink, C.H. Gierlich, I. Delidovich, R. Palkovits, Systematic catalyst screening of zeolites with various frameworks and Si/Al ratios to identify optimum acid strength in OME synthesis, Chem. Cat. Chem. 12 (2020) 5710.
[10] S.P. Lucas, F.L. Chan, G.M. Fioroni, T.D. Foust, A. Gilbert, J. Luecke, C. S. McEnally, J.A. Serdoncillo, A.J. Zdanowicz, J. Zhu, B. Windom, Fuel properties of oxymethylene ethers with terminating groups from methyl to butyl, Energy Fuels 36 (2022) 10213–10225.

[11] W. Leitner, J. Klankermayer, S. Pischinger, H. Pitsch, K. Kohse-Höinghaus, Advanced biofuels and beyond: chemistry solutions for propulsion and production, Angew. Chem. Int. Ed. 56 (2017) 5412.
[12] S.W. Benson, Pyrolysis of dimethyl Ether, J. Chem. Phys. 25 (1956) 27–31.
[13] P. Dagaut, J. Boettner, M. Cathonnet, Chemical kinetic study of dimethylether oxidation in a jet stirred reactor from 1 to 10 ATM: Experiments and kinetic modeling, Symp. (Int.) Combust. 26 (1996) 627–632.
[14] H.J. Curran, W.J. Pitz, C.K. Westbrook, P. Dagaut, J.C. Boettner, M. Cathonnet, A wide range modeling study of dimethyl ether oxidation, Int. J. Chem. Kinet. 30 (1997) 229–241.
[15] M.U. Alzueta, J. Muro, R. Bilbao, P. Glarborg, Oxidation of dimethyl ether and its interaction with nitrogen oxides, Isr. J. Chem. 39 (1999) 73–86.
[16] U. Burke, K.P. Somers, P. O'Toole, C.M. Zinner, N. Marquet, G. Bourque, E. L. Petersen, W.K. Metcalfe, Z. Serinyel, H.J. Curran, An ignition delay and kinetic modeling study of methane, dimethyl ether, and their mixtures at high pressures, Combust. Flame 162 (2015) 315–330.
[17] H. Hashemi, J.M. Christensen, P. Glarborg, High-pressure pyrolysis and oxidation of DME and DME/CH4, Combust. Flame 205 (2019) 80–92.
[18] M. Pelucchi, S. Schmitt, N. Gaiser, A. Cuoci, A. Frassoldati, H. Zhang, A. Stagni, P. Oßwald, K. Kohse-Höinghaus, T. Faravelli, On the influence of NO addition to dimethyl ether oxidation in a flow reactor, Combust. Flame 257 (2023) 112464.
[19] C. Zhang, P. Li, Y. Li, J. He, X. Li, Shock-tube study of dimethoxymethane ignition at high temperatures, Energy Fuels 28 (2014) 4603–4610.
[20] L. Marrodan, F. Monge, A. Millera, R. Bilbao, M. Alzueta, Dimethoxymethane oxidation in a flow reactor, Combust. Sci. Technol. 188 (2016) 719–729.
[21] E. Hu, Z. Gao, Y. Liu, G. Yin, Z. Huang, Experimental and modeling study on ignition delay times of dimethoxy methane/n-heptane blends, Fuel 189 (2017) 350–357.
[22] W. Sun, B. Yang, N. Hansen, K. Moshammer, The influence of dimethoxy methane (DMM)/dimethyl carbonate (DMC) addition on a premixed ethane/oxygen/argon flame, Proc. Combust. Inst. 36 (2017) 449–457.
[23] W. Sun, T. Tao, M. Lailliau, N. Hansen, B. Yang, P. Dagaut, Exploration of the oxidation chemistry of dimethoxymethane: Jet-stirred reactor experiments and kinetic modeling, Combust. Flame 193 (2018) 491–501.
[24] F.H. Vermeire, H. Carstensen, O. Herbinet, F. Battin-Leclerc, G.B. Marin, K.V. Van Geem, Experimental and modeling study of the pyrolysis and combustion of dimethoxymethane, Combust. Flame 190 (2018) 270–283.
[25] S. Jacobs, M. Döntgen, A. Alquaity, W.A. Kopp, L.C. Kröger, U. Burke, H. Pitsch, K. Leonhard, H.J. Curran, K.A. Heufer, Detailed kinetic modeling of dimethoxymethane. Part II: experimental and theoretical study of the kinetics and reaction mechanism, Combust. Flame 205 (2019) 522–533.
[26] K.P. Shrestha, S. Eckart, A.M. Elbaz, B.R. Giri, C. Fritsche, L. Seidel, W.L. Roberts, H. Krause, F. Mauss, A comprehensive kinetic model for dimethyl ether and dimethoxymethane oxidation and NOx interaction utilizing experimental laminar flame speed measurements at elevated pressure and temperature, Combust. Flame 218 (2020) 57–74.
[27] W. Sun, G. Wang, S. Li, R. Zhang, B. Yang, J. Yang, Y. Li, C.K. Westbrook, C. K. Law, Speciation and the laminar burning velocities of poly(oxymethylene) dimethyl ether 3 (POMDME3) flames: an experimental and modeling study, Proc. Combust. Inst. 36 (2017) 1269–1278.
[28] T. He, Z. Wang, X. You, H. Liu, Y. Wang, X. Li, X. He, A chemical kinetic mechanism for the low- and intermediate-temperature combustion of Polyoxymethylene Dimethyl Ether 3 (PODE3), Fuel 212 (2018) 223–235.
[29] H. Liu, Z. Wang, Y. Li, Y. Zheng, T. He, J. Wang, Recent progress in the application in compression ignition engines and the synthesis technologies of polyoxymethylene dimethyl ethers, Appl. Energy 233-234 (2019) 599–611.
[30] S. Drost, R. Schießl, M. Werler, J. Sommerer, U. Maas, Ignition delay times of polyoxymethylene dimethyl ether fuels (OME2 and OME3) and air: measurements in a rapid compression machine, Fuel 258 (2019) 116070.
[31] L. Cai, S. Jacobs, R. Langer, F. vom Lehn, K.A. Heufer, H. Pitsch, Auto-ignition of oxymethylene ethers (OMEn, $n = 2$–4) as promising synthetic e-fuels from renewable electricity: shock tube experiments and automatic mechanism generation, Fuel 264 (2020) 116711.
[32] K.P. Shrestha, S. Eckart, S. Drost, C. Fritsche, R. Schießl, L. Seidel, U. Maas, H. Krause, F. Mauss, A comprehensive kinetic modeling of oxymethylene ethers (OMEn, n=1–3) oxidation - laminar flame speed and ignition delay time measurements, Combust. Flame 246 (2022) 112426.
[33] J.M. Ngugi, S. Richter, M. Braun-Unkhoff, C. Naumann, U. Riedel, A study on fundamental combustion properties of oxymethylene ether-1, the primary reference fuel 90, and their blend: experiments and modeling, Combust. Flame 243 (2022) 111996.
[34] N. Gaiser, H. Zhang, T. Bierkandt, S. Schmitt, J. Zinsmeister, T. Kathrotia, P. Hemberger, S. Shaqiri, T. Kasper, M. Aigner, P. Oßwald, M. Köhler, Investigation of the combustion chemistry in laminar, low-pressure oxymethylene ether flames (OME0–4), Combust. Flame 243 (2022) 112060.
[35] N. Gaiser, T. Bierkandt, P. Oßwald, J. Zinsmeister, T. Kathrotia, S. Shaqiri, P. Hemberger, T. Kasper, M. Aigner, M. Köhler, Oxidation of oxymethylene ether (OME0−5): An experimental systematic study by mass spectrometry and photoelectron photoion coincidence spectroscopy, Fuel 313 (2022) 122650.
[36] Y. Hidaka, K. Sato, M. Yamane, High-temperature pyrolysis of dimethyl ether in shock waves, Combust. Flame 123 (2000) 1–22.
[37] S. Eckart, L. Cai, C. Fritsche, F. vom Lehn, H. Pitsch, H. Krause, Laminar burning velocities, CO, and NOx emissions of premixed polyoxymethylene dimethyl ether flames, Fuel 293 (2021) 120321.
[38] P. Dagaut, C. Daly, J.M. Simmie, M. Cathonnet, The oxidation and ignition of dimethylether from low to high temperature (500–1600 K): experiments and kinetic modeling, Symp. (Int.) Combust. 27 (1998) 361–369.
[39] H. Zhang, S. Schmitt, L. Ruwe, K. Kohse-Höinghaus, Inhibiting and promoting effects of NO on dimethyl ether and dimethoxymethane oxidation in a plug-flow reactor, Combust. Flame 224 (2021) 94–107.
[40] X. Zhong, H. Wang, Q. Zuo, Z. Zheng, J. Wang, W. Yin, M. Yao, Experimental and kinetic modeling studies of polyoxymethylene dimethyl ether (PODE) pyrolysis in jet stirred reactor, J. Anal. Appl. Pyrolysis 159 (2021) 105332.
[41] A. Stagni, S. Schmitt, M. Pelucchi, A. Frassoldati, K. Kohse-Höinghaus, T. Faravelli, Dimethyl ether oxidation analyzed in a given flow reactor: experimental and modeling uncertainties, Combust. Flame 240 (2022) 111998.
[42] Z. Qiu, A. Zhong, Z. Huang, D. Han, An experimental and modeling study on polyoxymethylene dimethyl ether 3 (PODE3) oxidation in a jet stirred reactor, Fundam. Res. 2 (2022) 738–747.
[43] K. De Ras, M. Kusenberg, J.W. Thybaut, K.M. Van Geem, Unraveling the carbene chemistry of oxymethylene ethers: Experimental investigation and kinetic modeling of the high-temperature pyrolysis of OME-2, Proc. Combust. Inst. 39 (2023) 125–133.
[44] H. Wang, Z. Yao, X. Zhong, Q. Zuo, Z. Zheng, Y. Chen, M. Yao, Experimental and kinetic modeling studies on low-temperature oxidation of Polyoxymethylene Dimethyl Ether (DMM1-3) in a jet-stirred reactor, Combust. Flame 245 (2022) 112332.
[45] T.A. Cool, J. Wang, N. Hansen, P.R. Westmoreland, F.L. Dryer, Z. Zhao, A. Kazakov, T. Kasper, K. Kohse-Höinghaus, Photoionization mass spectrometry and modeling studies of the chemistry of fuel-rich dimethyl ether flames, Proc. Combust. Inst. 31 (2007) 285–293.
[46] G. Chen, W. Yu, J. Fu, J. Mo, Z. Huang, J. Yang, Z. Wang, H. Jin, F. Qi, Experimental and modeling study of the effects of adding oxygenated fuels to premixed n-heptane flames, Combust. Flame 159 (2012) 2324–2335.
[47] H. Zhang, D. Kaczmarek, C. Rudolph, S. Schmitt, N. Gaiser, P. Oßwald, T. Bierkandt, T. Kasper, B. Atakan, K. Kohse-Höinghaus, Dimethyl ether (DME) and dimethoxymethane (DMM) as reaction enhancers for methane: combining flame experiments with model-assisted exploration of a polygeneration process, Combust. Flame 237 (2022) 111863.
[48] T. Kathrotia, P. Oßwald, C. Naumann, S. Richter, M. Kohler, Combustion kinetics of alternative jet fuels, Part-II: Reaction model for fuel surrogate, Fuel 302 (2021) 120736.
[49] T. Kathrotia, P. Oßwald, J. Zinsmeister, T. Methling, M. Kohler, Combustion kinetics of alternative jet fuels, Part-III: fuel modeling and surrogate strategy, Fuel 302 (2021) 120737.
[50] P. Glarborg, J.A. Miller, B. Ruscic, S.J. Klippenstein, Modeling nitrogen chemistry in combustion, Prog. Energy Combust. Sci. 67 (2018) 31–68.
[51] M. Köhler, P. Oßwald, H. Xu, T. Kathrotia, C. Hasse, U. Riedel, Speciation data for fuel-rich methane oxy-combustion and reforming under prototypical partial oxidation conditions, Chem. Eng. Sci. 139 (2016) 249–260.
[52] P. Oßwald, R. Whitside, J. Schäffer, M. Köhler, An experimental flow reactor study of the combustion kinetics of terpenoid jet fuel compounds: Farnesane, p-menthane and p-cymene, Fuel 187 (2017) 43–50.
[53] T. Kathrotia, P. Oßwald, M. Kohler, N. Slavinskaya, U. Riedel, Experimental and mechanistic investigation of benzene formation during atmospheric pressure flow reactor oxidation of n-hexane, n-nonane, and n-dodecane below 1200 K, Combust. Flame 194 (2018) 426–438.
[54] P. Oßwald, J. Zinsmeister, T. Kathrotia, M. Alves-Fortunato, V. Burger, R. van der Westhuizen, C. Viljoen, K. Lehto, R. Sallinen, K. Sandberg, M. Aigner, P.L. Clercq, M. Köhler, Combustion kinetics of alternative jet fuels, Part-I: experimental flow reactor study, Fuel 302 (2021) 120735.
[55] B. Lumpp, D. Rothe, C. Pastötter, R. Lämmermann, E. Jacob, Oxymethylene ethers as diesel fuel additives of the future, MTZ Worldw 72 (2011) 34–38.
[56] J. Liu, H. Wang, Y. Li, Z. Zheng, Z. Xue, H. Shang, M. Yao, Effects of diesel/PODE (polyoxymethylene dimethyl ethers) blends on combustion and emission characteristics in a heavy duty diesel engine, Fuel 177 (2016) 206–216.
[57] A. Omari, B. Heuser, S. Pischinger, Potential of oxymethylenether-diesel blends for ultra-low emission engines, Fuel 209 (2017) 232–237.
[58] C.K. Westbrook, W.J. Pitz, H.J. Curran, Chemical kinetic modeling study of the effects of oxygenated hydrocarbons on soot emissions from diesel engines, J. Phys. Chem. A 110 (2006) 6912–6922.
[59] M. Härtl, P. Seidenspinner, E. Jacob, G. Wachtmeister, Oxygenate screening on a heavy-duty diesel engine and emission characteristics of highly oxygenated oxymethylene ether fuel OME1, Fuel 153 (2015) 328–335.
[60] C. Barro, M. Parravicini, K. Boulouchus, A. Liati, Neat polyoxymethylene dimethyl ether in a diesel engine; part 2: exhaust emission analysis, Fuel 234 (2018) 1414–1421.
[61] D. Pelerin, K. Gaukel, M. Härtl, E. Jacob, G. Wachtmeister, Potentials to simplify the engine system using the alternative diesel fuels oxymethylene ether OME1 and OME3−6 on a heavy-duty engine, Fuel 259 (2020) 116231.
[62] J. Burger, M. Siegert, E. Ströfer, H. Hasse, Poly(oxymethylene) dimethyl ethers as components of tailored diesel fuel: properties, synthesis and purification concepts, Fuel 89 (2010) 3315–3319.
[63] J.M. Ngugi, A Study on Auto-Ignition of poly(oxymethylene) Dimethyl Ethers and Their Mixtures with the Primary Reference Fuel 90, PhD Thesis 07.03.2023, University of Stuttgart, Germany. https://doi.org/10.18419/opus-13449.
[64] F. Lindner, M. Braun-Unkhoff, C. Naumann, T. Kathrotia, M. Köhler, U. Riedel, An Experimental speciation study on the pyrolysis and oxidation of the oxygenated fuels DME, OME1, and OME2 in a single pulse shock tube, in: Proc. 11th ECM, 2023. https://ecm2023.sciencesconf.org/.

[65] S. Richter, T. Kathrotia, M. Braun-Unkhoff, C. Naumann, M. Köhler, Influence of oxymethylene ethers (OMEn) in mixtures with a diesel surrogate, Energies 14 (2021) 7848.

[66] J.M. Ngugi, S. Richter, M. Braun-Unkhoff, C. Naumann, M. Köhler, U. Riedel, A study on fundamental combustion properties of Oxymethylene Ether-2, ASME J. Eng. Gas Turbines Power 144 (2022) 011014.

[67] K. Wang, R. Xu, T. Parise, J. Shao, A. Movaghar, D.J. Lee, J. Park, Y. Gao, T. Lu, F. N. Egolfopoulos, D.F. Davidson, R.K. Hanson, C.T. Bowman, H. Wang, A physics-based approach to modeling real-fuel combustion chemistry – IV. HyChem modeling of combustion kinetics of a bio-derived jet fuel and its blends with a conventional Jet A, Combust. Flame 198 (2018) 477–489.

[68] A. Rodriguez, O. Frottier, O. Herbinet, R. Fournet, R. Bounaceur, C. Fittschen, F. Battin-Leclerc, Experimental and modeling investigation of the low-temperature oxidation of Dimethyl Ether, J. Phys. Chem. A 119 (2015) 7905–7923.

[69] K. De Ras, M. Kusenberg, G. Vanhove, Y. Fenard, A. Eschenbacher, R.J. Varghese, J. Aerssens, R. Van de Vijver, L. Tran, J.W. Thybaut, K.M. Van Geem, A detailed experimental and kinetic modeling study on pyrolysis and oxidation of oxymethylene ether-2 (OME-2), Combust. Flame 238 (2022) 111914.

[70] R. Sivaramakrishnan, J.V. Michael, A.F. Wagner, R. Dawes, A.W. Jasper, L. B. Harding, Y. Georgievskii, S.J. Klippenstein, Roaming radicals in the thermal decomposition of dimethyl ether: experiment and theory, Combust. Flame 158 (2011) 618–632.

[71] H.J. Curran, S.L. Fischer, F.L. Dryer, The reaction kinetics of dimethyl ether. II: low-temperature oxidation in flow reactors, Int. J. Chem. Kinet. 32 (2000) 741–759.

[72] T. Yu, X. Wu, X. Zhou, A. Bodi, P. Hemberger, Hydrogen migration as a potential driving force in the thermal decomposition of dimethoxymethane: New insights from pyrolysis imaging photoelectron photoion coincidence spectroscopy and computations, Combust. Flame 222 (2020) 123–132.

[73] K. Yasunaga, F. Gillespie, J.M. Simmie, H.J. Curran, Y. Kuraguchi, H. Hoshikawa, M. Yamane, Y. Hidaka, A multiple shock tube and chemical kinetic modeling study of diethyl ether pyrolysis and oxidation, Phys. Chem. A 114 (2010) 9098–9109.

[74] F.R. Gillespie, An experimental and Modelling Study of the Combustion of Oxygenated Hydrocarbons. PhD Thesis, publication date 19-03-2014, NUI University of Galway. http://hdl.handle.net/10379/4419.

[75] X. Qin, Y. Ju, Measurements of burning velocities of dimethyl ether and air premixed flames at elevated pressures, Proc. Combust. Inst. 30 (2005) 233–240.

[76] J. de Vries, W.B. Lowry, Z. Serinyel, H.J. Curran, E.L. Petersen, Laminar flame speed measurements of dimethyl ether in air at pressures up to 10atm, Fuel 90 (2011) 331–338.

[77] M.L. Lavadera, C. Brackmann, A.A. Konnov, Laminar burning velocities and nitric oxide formation in premixed dimethyl ether/air flames: experiments and kinetic modeling, Combust. Flame 246 (2022) 112411.

[78] Q. Wang, W. Sun, L. Guo, S. Lin, P. Cheng, H. Zhang, Y. Yan, Experimental and kinetic study on the laminar burning speed, Markstein length and cellular instability of oxygenated fuels, Fuel 297 (2021) 120754.

[79] K. Moshammer, A.W. Jasper, D.M. Popolan-Vaida, Z. Wang, V. Shankar, L. Ruwe, C.A. Taatjes, P. Dagaut, N. Hansen, Quantification of the Keto-Hydroperoxide (HOOCH2OCHO) and other elusive intermediates during low-temperature oxidation of dimethyl ether, J. Phys. Chem. A 120 (2016) 7890–7901.

[80] K. De Ras, T. Panaget, Y. Fenard, J. Aerssens, L. Pillier, J.W. Thybaut, G. Vanhove, K.M. Van Geem, An experimental and kinetic modeling study on the low-temperature oxidation of oxymethylene ether-2 (OME-2) by means of stabilized cool flames, Combust. Flame 253 (2023) 112792.

[81] M. Zeng, J. Wullenkord, I. Graf, K. Kohse-Höinghaus, Influence of dimethyl ether and diethyl ether addition on the flame structure and pollutant formation in premixed iso-octane flames, Combust. Flame 184 (2017) 41–54.

[82] P. Oßwald, M. Köhler, An atmospheric pressure high-temperature laminar flow reactor for investigation of combustion and related gas phase reaction systems, Rev. Sci. Instrum. 86 (2015) 105–109.

[83] P. Dagaut, M. Reuillon, M. Cathonnet, High pressure oxidation of liquid fuels from low to high temperature. 2. mixtures of n-heptane and iso-octane, Combust. Sci. Technol. 103 (1994) 315–336.

[84] D.R. Haylett, P.P. Lappas, D.F. Davidson, R.K. Hanson, Application of an aerosol shock tube to the measurement of diesel ignition delay times, Proc. Combust. Inst. 32 (2009) 477–484.

[85] K. Mati, A. Ristori, S. Gail, G. Pengloan, P. Dagaut, The oxidation of a diesel fuel at 1–10 atm: experimental study in a JSR and detailed chemical kinetic modeling, Proc. Combust. Inst. 31 (2007) 2939–2946.

[86] R. Schmitz, C. Russo, F. Ferraro, B. Apicella, C. Hasse, M. Sirignano, Effect of oxymethylene ether-2-3-4 (OME2-4) on soot particle formation and chemical features, Fuel 324 (2022) 124617.

[87] H. Wang, R. Fang, B.W. Weber, C. Sung, An experimental and modeling study of dimethyl ether/methanol blends autoignition at low temperature, Combust. Flame 198 (2018) 89–99.

[88] W. Ying, L. Genbao, Z. Wei, Z. Longbao, Study on the application of DME/diesel blends in a diesel engine, Fuel. Process. Technol. 89 (2008) 1272–1280.

[89] M.C. Lee, S.B. Seo, J.H. Chung, Y.J. Joo, D.H. Ahn, Industrial gas turbine combustion performance test of DME to use as an alternative fuel for power generation, Fuel 88 (2009) 657–662.

[90] M.C. Lee, Y. Yoon, Development of a gas turbine fuel nozzle for DME and a design method thereof, Fuel 102 (2012) 823–830.

[91] E.E. Dames, A.S. Rosen, B.W. Weber, C.W. Gao, C. Sung, W.H. Green, A detailed combined experimental and theoretical study on dimethyl ether/propane blended oxidation, Combust. Flame 168 (2016) 310–330.

[92] T. Amano, F.L. Dryer, Effect of dimethyl ether, NOx, and ethane on CH4 oxidation: High pressure, intermediate-temperature experiments and modeling, Symp. (Int.) Combust. 27 (1998) 397–404.

[93] Z. Chen, X. Qin, Y. Ju, Z. Zhao, M. Chaos, F.L. Dryer, High temperature ignition and combustion enhancement by dimethyl ether addition to methane–air mixtures, Proc. Combust. Inst. 31 (2007) 1215–1222.

[94] Z. Hong, D. Davidson, R. Hanson, Shock tube studies of soot formation in heptane and heptane/dme mixtures, in: 45th AIAA Aerospace Sciences Meeting and Exhibit, 2007. AIAA 2007-774.

[95] C. Tang, L. Wei, J. Zhang, X. Man, Z. Huang, Shock tube measurements and kinetic investigation on the ignition delay times of methane/dimethyl ether mixtures, Energy Fuels 26 (2012) 6720–6728.

[96] X. Jiang, Z. Tian, Y. Zhang, Z. Huang, Shock tube measurement and simulation of DME/n-butane/air mixtures: effect of blending in the NTC region, Fuel 203 (2017) 316–329.

[97] Y. Zhang, K.P. Somers, M. Mehl, W.J. Pitz, R.F. Cracknell, H.J. Curran, Probing the antagonistic effect of toluene as a component in surrogate fuel models at low temperatures and high pressures. A case study of toluene/dimethyl ether mixtures, Proc. Combust. Inst. 36 (2017) 413–421.

[98] X. Jiang, F. Deng, F. Yang, Z. Huang, Ignition delay characteristics and kinetic investigation of dimethyl ether/n-pentane binary mixtures: interpreting the effect of the equivalence ratio and dimethyl ether blending, Energy Fuels 32 (2018) 3814–3823.

[99] J. Herzler, M. Fikri, C. Schulz, High-pressure shock-tube study of the ignition and product formation of fuel-rich dimethoxymethane (DMM)/air and CH4/DMM/air mixtures, Combust. Flame 216 (2020) 293–299.

[100] L. Lu, C. Zou, Q. Lin, Y. Liu, H. Jing, Experimental and simulated study on the ignition delay time of dimethyl ether/n-heptane/oxygen/argon mixtures, Fuel 264 (2020) 116812.

[101] S. Porras, D. Kaczmarek, J. Herzler, S. Drost, M. Werler, T. Kasper, M. Fikri, R. Schießl, B. Atakan, C. Schulz, U. Maas, An experimental and modeling study on the reactivity of extremely fuel-rich methane/dimethyl ether mixtures, Combust. Flame 212 (2020) 107–122.

[102] P. Dagaut, F. Lecomte, S. Chevailler, M. Cathonnet, Mutual sensitization of the oxidation of nitric oxide and simple fuels over an extended temperature range: experimental and detailed kinetic modeling, Combust. Sci. Technol. 148 (1999) 27–57.

[103] T. Faravelli, A. Frassoldati, E. Ranzi, Kinetic modeling of the interactions between NO and hydrocarbons in the oxidation of hydrocarbons at low temperatures, Combust. Flame 132 (2003) 188–207.

[104] J.H. Bromly, F.J. Barnes, S. Muris, X. You, B.S. Haynes, Kinetic and thermodynamic sensitivity analysis of the NO-sensitised oxidation of methane, Combust. Sci. Technol. 115 (1996) 259–296.

[105] P. Dagaut, J. Luche, M. Cathonnet, The low temperature oxidation of DME and mutual sensitization of the oxidation of DME and nitric oxide: experimental and detailed kinetic modeling, Combust. Sci. Technol. 165 (2001) 61–84.

[106] W. Ye, J.C. Shi, R.T. Zhang, X.J. Wu, X. Zhang, M.L. Qi, S.N. Luo, Experimental and kinetic modeling study of CH_3OCH_3 ignition sensitized by NO_2, Energy Fuels 30 (2016) 10900.

[107] L. Dai, H. Hashemi, P. Glarborg, S. Gersen, P. Marshall, A. Mokhov, H. Levinsky, Ignition delay times of NH3 /DME blends at high pressure and low DME fraction: RCM experiments and simulations, Combust. Flame 227 (2021) 120–134.

[108] G. Issayev, B.R. Giri, A.M. Elbaz, K.P. Shrestha, F. Mauss, W.L. Roberts, A. Farooq, Ignition delay time and laminar flame speed measurements of ammonia blended with dimethyl ether: a promising low carbon fuel blend, Renew. Energy 181 (2022) 1353–1370.